Peer reviewed version

Link to published version (if available):
10.1016/j.earscirev.2019.102961

Link to publication record in Explore Bristol Research
PDF-document

University of Bristol - Explore Bristol Research
General rights

1   **Climatic and environmental changes across the Early Eocene Climatic Optimum at mid-**

2   **Waipara River, Canterbury Basin, New Zealand**

3

4   E.M. Crouch[1], C.L. Shepherd[1], H.E.G. Morgans[1], B.D.A. Naafs[2], E. Dallanave[3], A. Phillips[1], C.J.

5   Hollis[1], R.D. Pancost[2]

6   [1]GNS Science, P.O. Box 30368, Lower Hutt, New Zealand

7   [2]Organic Geochemistry Unit, School of Chemistry, School of Earth Sciences, and Cabot Institute for

8   the Environment, University of Bristol, UK

9   [3]Research Group Marine Geophysics, Faculty of Geosciences, University of Bremen, GEO Gebäude,

10   Klagenfurter Straße, 28359 Bremen, Germany

Abstract

11

12   The Cretaceous–Paleogene marine sedimentary succession exposed in the banks of the middle

13   reaches of the Waipara River (referred to as mid-Waipara), north Canterbury, New Zealand, has been

14   the subject of several high-profile studies of Paleogene paleoclimate over the past decade. It is one of

15   relatively few sections globally where a multi-proxy approach is possible due to the good preservation

16   of microfossils and organic biomarkers. The Eocene section is also well dated by magnetostratigraphy

17   and biostratigraphy based on planktic foraminifera, calcareous nannofossils and dinoflagellate cysts

18   (dinocysts). Here, we build on this previous work and undertake a comprehensive analysis of

19   paleontological and geochemical indicators of climatic and environmental changes through the early–

20   middle Eocene part of the section, with particular focus on the Early Eocene Climatic Optimum

21   (EECO; 53.26–49.14 Ma). We correlate a 33.5 m-thick interval with the EECO, based on

22   biostratigraphy, magnetostratigraphy, TEX_{86}-paleothermometry and bulk carbonate $\delta^{13}C$. Our new

23   sea-surface temperature (SST) record based on TEX_{86} agrees with a previous lower resolution record

24   based on TEX_{86} and planktic foraminiferal $\delta^{18}O$ and Mg/Ca ratios. The EECO interval in this section

25   extends from the upper part of the New Zealand Waipawan Stage to the Mangaorapan/Heretaungan

26   Stage boundary at 49.27 Ma. The EECO onset is not exposed, but the termination is well constrained

27   by a fall in SST and shift to more positive $\delta^{13}C$ values. Six negative carbon isotope excursions (CIEs)

28   are recognised within the EECO and are tentatively correlated with CIEs J/K, M, O, Q, T and C22nH4

29   in the global $\delta^{13}C$ compilation. The CIEs are associated with warmer SSTs, indicating that they

30   represent hyperthermals. The BAYSPAR TEX_{86} calibration indicates SST increased by as much as

31   12°C from the early Eocene (~55 Ma) to the EECO, where SST peaked at 35°C. SST gradually

32   declined from mid EECO (~51 Ma) into the middle Eocene. The marked warming in the early EECO

33   is associated with the highest abundance of warm-water taxa in calcareous nannofossil and dinocyst

34   assemblages, the highest proportion of planktic foraminifera, and a coeval long-term shift to abundant

35   angiosperm vegetation, primarily driven by a rise in Casuarinaceae. There is good agreement between

36   TEX_{86} and marine microfossil-based proxies for temperature, providing confidence that both

37   approaches are useful guides to past water temperature. Warm-water marine taxa are most abundant in

38   the EECO but are not dominant. Comparison of the abundance of nannofossil warm-water taxa

39   between mid-Waipara and a low-latitude site on Shatsky Rise suggests the latitudinal temperature

40   gradient between mid- and low-latitudes in the EECO was greater than the TEX_{86} proxy implies.

41   There is no clear evidence for enhanced sedimentation rates associated with the EECO, in contrast to

42   evidence from the nearby Mead Stream section. Superabundant *Homotryblium*, a euryhaline dinocyst,

43   in the early and middle EECO suggests elevated salinity and/or stratified surface waters, and there is

44   no clear evidence of increased surface productivity associated with the EECO. Declining SST in the

45   late EECO, ~50 Ma, corresponds with an increase in cool-water taxa and terrigenous material. This

46   article highlights the importance of combining well-calibrated paleontological and geochemical

47   records to better constrain and understand past warm climate states.

48

1. Introduction

A succession of short- and long-term global warming events during the early Eocene (56–48 Ma) provide important insights into climate variability under background conditions of elevated atmospheric CO_2, generally exceeding 800 ppmv (Zachos et al., 2008; Anagnostou et al., 2016; Hollis et al., 2019). Well-calibrated sedimentary records for this time period from different regions are essential to understand the geographic variability in climate and ecosystem response and to validate Earth system models (Huber and Cabellero, 2011; Lunt et al., 2017). Records from the South Pacific are of particular interest because the Pacific Ocean was the primary driver of ocean heat transport during the Paleogene (Huber and Nof, 2006). Both model and proxy studies indicate that the Pacific sector of the Southern Ocean was a major source of deep water through most of the Paleogene (Littler et al., 2014; Huck et al., 2017). For this reason, the Southwest Pacific has been the focus of several studies of early Paleogene climate dynamics over the past two decades (e.g., Crouch et al. 2003; Nicolo et al., 2007; Bijl et al., 2009, 2013a; Hollis et al., 2009, 2012, 2015; Slotnick et al., 2012, 2015; Pancost et al., 2013; Taylor et al., 2013; Dallanave et al., 2014, 2016; Inglis et al., 2015; Hines et al., 2017; Naafs et al., 2018).

The lower Paleogene succession at mid-Waipara River, Canterbury Basin, New Zealand (Fig. 1), has been a focus of many of these studies because the siliciclastic sediments contain a wide range of microfossils as well as immature organic matter suitable for biomarker studies. Studies have investigated both marine and terrestrial temperature records from latest Cretaceous to middle Eocene, focusing on glycerol dialkyl glycerol tetraethers (GDGTs; Hollis et al., 2009, 2012, 2014; Pancost et al., 2013; Taylor et al., 2013, 2018) as well as Mg/Ca ratios and oxygen isotopes (Hollis et al. 2009, 2012; Creech et al. 2010; Hines et al., 2017). These studies have provided multiproxy estimates of temperature, which have been compared with climate and general circulation models (Huber and Caballero, 2011; Hollis et al., 2012; Lunt et al., 2012). The Eocene section also has a well-calibrated age model that incorporates dinocyst, foraminiferal and nannofossil biostratigraphy and magnetostratigraphy (Dallanave et al. 2016; Shepherd and Kulhanek, 2016). Whilst paleontology has supported these studies, the focus has been on biostratigraphy rather than paleontological indicators of

climatic and environmental change in the Eocene greenhouse world. In this article, we utilise the well-preserved calcareous and organic-walled microfossil assemblages in this continental margin section to evaluate proxy- and model-based climate reconstructions and to infer the biological response to changes in climate and carbon cycling.

Our multidisciplinary study includes analysis of foraminiferal, calcareous nannofossil, dinoflagellate cyst (dinocyst) and spore/pollen assemblages, bulk carbonate $\delta^{13}C$ isotopes, $CaCO_3$ content, and biomarkers (GDGTs), and utilises samples collected as part of our magnetostratigraphic study (Dallanave et al., 2016) of the lower and middle Eocene succession at mid-Waipara River. We document the timing and variability of environmental and climatic changes in the marine and terrestrial realm, and compare these changes with a new and more detailed record of sea surface temperature (SST) and carbon cycle change than has been previously reported for this section.

2. Identifying the Early Eocene Climatic Optimum (EECO)

The warmest sustained temperatures of the Cenozoic occurred in the EECO (Zachos et al., 2001, 2008; Westerhold and Röhl, 2009; Lauretano et al., 2016; Evans et al., 2018) and were associated with atmospheric CO_2 levels of >800 ppmv (Beerling and Royer, 2011; Anagnostou et al., 2016; Boudreau et al., 2019; Hollis et al., 2019). The EECO (Fig. 2) was initially defined by a minimum in oxygen isotope ($\delta^{18}O$) values of benthic foraminifera that lasted 2–3 Myrs, from ~53–50 Ma (Zachos et al., 2001; Kirtland Turner, 2014). Recent studies indicate that the EECO onset can be tied to one of several carbon isotope excursions (CIEs) from the middle early Eocene (Cramer et al., 2003; Westerhold et al., 2012; Lauretano et al., 2015, 2018). A new astronomically-tuned, benthic foraminiferal record at ODP Site 1209, North Pacific, recommends that the J event, dated at 53.26 Ma, be adopted as the base of the EECO (Westerhold et al., 2018). In the hemipelagic succession of eastern Marlborough, New Zealand (Fig. 1), this CIE coincides with a transition from limestone to marl-dominated sediments (Hollis et al., 2005 a, b), which is inferred to reflect hydrological changes linked to the EECO (Slotnick et al, 2012, 2015; Dallanave et al., 2014). The top of the EECO is tied to

102 a CIE in uppermost Chron C22n (C22nH5), dated at 49.14 Ma, that is coincident with the onset of a

103 long-term cooling trend in the benthic $\delta^{18}O$ record (Westerhold et al., 2018).

104 Thus, the EECO is currently considered to extend from 53.26 Ma to 49.14 Ma, Chron

105 C24n.2rH1 (J event) to uppermost Chron C22n (CIE C22nH5), an interval of 4.12 Myrs that extends

106 from the upper part of calcareous nannofossil zone NP11 to lower NP14 (Hollis et al., 2019). In terms

107 of New Zealand stages (Raine et al., 2015), the EECO extends from the late Waipawan to close to the

108 Mangaorapan/Heretaungan boundary (49.27 Ma) and includes the Waipawan/Mangaorapan boundary

109 at 52 Ma (Fig 2).

110

111 **3. Previous early to middle Eocene studies at mid-Waipara River**

112 The lower–middle Eocene Ashley Mudstone succession outcrops along the river bed (Fig. 1),

113 and three sample suites have been collected (Supp. Information Fig. 1). Two suites, from 2003 and

114 2007, are integrated into one composite section (Morgans et al., 2005) and have been the focus of

115 several studies, including $\delta^{13}C$ isotopes, Mg/Ca ratios, GDGT analyses, and biostratigraphy (Hollis et

116 al., 2009, 2012; Creech et al., 2010; Pancost et al., 2013; Taylor et al., 2013; Inglis et al., 2015). As

117 part of a magnetostratigraphic study (Dallanave et al., 2016), a third suite was taken in 2012 (Fig. 3)

118 from the same river bed section as the 2003 collection. Oriented samples for paleomagnetic analyses

119 were taken over a ~45 m stratigraphic interval. Six magnetic polarity reversals were correlated to

120 magnetic polarity Chrons C23n.2n to C21 n, with the aid of nannofossil and foraminiferal

121 biostratigraphy. This correlation spans from ~51.5–47 Ma, based on the orbitally-tuned Eocene

122 timescale of Westerhold et al. (2017), and provides a magnetostratigraphically calibrated age for the

123 base of the NZ Heretaungan Stage, i.e., 49.27 Ma (C22n(0.6)).

124 Following the recommendation of van Hinsbergen et al. (2015), our paleogeographic

125 reconstruction (Fig. 1) and Eocene locations of the sites mentioned in the text are based on a

126 paleomagnetic reference frame (Matthews et al., 2016). This reference frame is more suitable than a

127 mantle-based reference frame for paleoceanographic and paleoclimate studies because it is tied to the

128 Earth's spin axis and therefore more accurately represents true paleolatitude. As noted by van

129 Hinsbergen et al. (2015), this change in reference frame moves Southwest Pacific Paleogene sites

130 northward by ~10° and the mid-Waipara site shifts from the previously reported paleolatitude of 55°S

131 (e.g. Hollis et al., 2009, 2012) to 46°S (Fig. 1).

132

133 **4. Material and methods**

134 *4.1 Mid-Waipara River section and samples*

135   The mid-Waipara River section (Fig. 1) is situated ~13 km west of the Waipara township,

136 north Canterbury, and includes the area downstream from Doctors Gorge to top of the Amuri

137 Limestone in what is referred to as the 'lower gorge' (NZ Map Series 260, reference M34/755 946–

138 M34/789 944). The Ashley Mudstone comprises low-dipping calcareous mudstone outcropping in the

139 river bed (Morgans et al., 2005). Strata are well-exposed in the central part, but exposure is more

140 variable in the upper and lower parts, and highly dependent on river level and sediment load. Samples

141 are examined from two suites, the 2007 and 2012 collections (Fig. 3; Supp. Information Fig. 1). The

142 two collections are correlated by biostratigraphy and lithology, as the reference marker used in the

143 2007 collection was washed away and direct field correlation was not possible. The base of the 2012

144 (M34/f930) and top of the 2007 (M34/f889) collections are inferred to be separated by a stratigraphic

145 gap of ~1 m. Eleven samples (M34/f899–f889) were collected in 2007 from ~15 m of stratigraphic

146 section, although the middle part of the section (-13.2 to -6.6 m) could not be sampled as the river

147 level was too high. In 2012, a detailed suite of 118 samples (M34/f930–f1047) were taken from ~66.5

148 m of section.

149

150 *4.2 Microfossils*

151   Biostratigraphic and paleoenvironmental studies were completed for foraminifera, calcareous

152 nannofossils, dinocysts, and spores and pollen. All paleontological samples, residues and slides are

153   stored in the National Paleontological Collection at GNS Science, Lower Hutt, NZ. Biostratigraphic

154   data are in the Appendix (Supp. Information).

155

156   *4.2.1 Foraminifera*

157   A total of 92 samples were processed, with 500 g of dried sediment washed over a 75 μm

158   screen for each sample. The residues were then dried, reweighed and half was retained for a

159   quantitative census. The remaining half of the residues were qualitatively picked to obtain a

160   comprehensive faunal assemblage that was used for biostratigraphy and paleodepth. A subsequent

161   count was completed to calculate the planktic/benthic foraminiferal ratio, and this value is expressed

162   as the proportion of planktic specimens in the total foraminiferal assemblage (planktic abundance).

163

164   *4.2.2 Calcareous nannofossils*

165   Smear slides were made for 34 samples using standard techniques (Bown and Young, 1998).

166   In some cases, samples contained a large amount of fine sand and strewn slides were prepared

167   according to the method of Bown and Young (1998). Slides were analysed using an Olympus BX53

168   microscope at 1000x magnification in plane-transmitted light (PL), cross-polarized light (XPL) and

169   phase contrast (PC) light. Relative abundance of taxa was determined from counts of 450 specimens

170   along random traverses of each slide, followed by scanning to identify additional rare species.

171   Specimens were identified to species level following the taxonomic concepts of Perch-Nielsen (1985),

172   Bown (1998, 2005), Dunkley Jones et al. (2009) and Shamrock and Watkins (2012). Results are

173   correlated to the zonation scheme of Martini (1971), with subzones as defined by Aubry (1991) and

174   absolute ages for events calibrated to Gradstein et al. (2012) and Hollis et al. (2019). Full synonymies

175   for all taxa mentioned in this paper are available in the publications listed above. To examine

176   paleotemperature changes, we distinguish cool- and warm-water taxa based on previous studies that

177   use statistical analyses of assemblage data (e.g., cluster analysis, principal component analysis) to

178   interpret patterns and relationships among taxa (e.g. Wei and Wise, 1990; Siesser, 1993; Bralower,

179   2002; Villa and Persico, 2006; Villa et al., 2008; Schneider et al., 2011; Shamrock and Watkins,

180   2012). Cool-water taxa comprise *Chiasmolithus* spp. and *Reticulofenestra daviesii*, while warm-water

181   taxa comprise *Discoaster* spp., *Sphenolithus* spp. and *Coccolithus formosus*.

182

183   *4.2.3. Palynomorphs*

184   A total of 45 samples were processed using standard palynological processing techniques.

185   Between 21 and 31 g of sediment was crushed, dried and the carbonate and siliceous component

186   removed by adding 10% HCl and 50% HF, respectively. Samples were oxidised, for up to 10 minutes,

187   using 70% HNO_3 and washed with 5% NH_4OH to disaggregate amorphous and organic debris. Some

188   samples were placed in an ultrasonic bath (for up to 1 minute) prior to sieving. All samples were

189   sieved over a 6 μm mesh, and well-mixed representative fractions of the >6 μm residue mounted on

190   glass slides using a glycerine jelly medium. The relative abundance of palynomorphs was determined

191   in three ways; 1) ~200 dinocysts counted for 43 samples, 2) ~ 200 spores/pollen counted for 33

192   samples, and 3) ~150 marine and terrestrial palynomorphs counted for 37 samples. At least one extra

193   slide was scanned for additional rare species. Quantitative results are shown as a percentage of the

194   total count, or with reference to the following: rare (1–5%), common (6–10%), frequent (11–20%),

195   abundant (21–40%) and super abundant (>40%). Dinocyst biostratigraphy is correlated to the

196   established New Zealand zonation (Morgans et al., 2004), with early Eocene zones based on Crouch

197   (2001; Fig. 2). An alternative South Pacific zonation (Bijl et al., 2013a) is not utilised because several

198   index species are either not present at mid-Waipara (e.g., lowest occurrence (LO) of *Arachnodinium*

199   *antarcticum*) or seem to have diachronous ranges (e.g. highest occurrence (HO) of *Palaeocystodinium*

200   *golzowense* is older in New Zealand than recorded at ODP Site 1172, East Tasman Plateau).

201   To examine paleotemperature changes, we distinguish taxa with a low-latitude (warm-water)

202   affinity from those with a Southern Ocean (cooler-water) affinity. Our warm-water group includes

203   taxa of the Wetzlielloideae subfamily: *Apectodinium*, *Charelsdowniea*, *Dracodinium*,

204   *Rhombodinium*, *Wetzeliella* and *Wilsonidium*. The genus *Apectodinium* evolved in equatorial regions,

205   with a LO close to the Danian/Selandian boundary (~61 Ma, Guasti et al., 2005; Awad and Oboh-

Ikuenobe, 2016), while other Wetzelielloideae taxa (*Rhombodinium*, *Wilsonidium*) have LOs in north-east India (Prasad et al., 2006) and the Tethys (Iakovleva and Heilmann-Clausen, 2007) in sediments dated as latest Paleocene. Recent work suggests the lower SST tolerance of Wetzelielloideae was $20 \pm 2.5°C$ (Frieling et al., 2014). The genus *Homotryblium* also evolved in low latitudes, with a LO near the base of the Thanetian (upper Foraminifera Zone P4a, Iakovleva et al., 2001; Crouch et al., 2003; Slimani et al., 2016). We keep the *Homotryblium* genus separate from the Wetzelielloideae group as it has a different morphology and may have had a broader SST range, from tropical–warm temperate (Köthe, 1990; Brinkhuis, 1994), although a recent study suggests it is part of an epicystal Goniodomideae ecogroup that preferred SSTs $>25 \pm 2.5°C$ (Frieling and Sluijs, 2018). Taxa associated with the Endemic Antarctic Community (EAC), or transantarctic community (Wrenn and Beckman, 1982; Bijl et al., 2011), are found south of ~45°S (Bijl et al., 2013b) and may have preferred cooler Antarctica-derived surface currents, particularly in the late early Eocene–late Eocene (Bijl et al., 2011, 2013b). In this study we identify a limited number of EAC taxa, comprising *Alterbidinium assymetricum*, *Deflandrea antarctica*, *Enneadocysta* group and *Spinidinium macmurdoense*. Whilst Bijl et al. (2013b) considered *Membranophoridium perforatum* to be part of the EAC, we do not include this taxon as it appears to have extended north of 45°S in some regions (Wilson, 1988).

4.3 Stable isotopes and carbonate content

A total of 68 samples were analysed for carbonate content and bulk carbonate $\delta^{13}C$ and $\delta^{18}O$ at the National Isotope Centre, GNS Science. Samples were analysed on the GVI IsoPrime Preparation System at a reaction temperature of 25°C for 24 hours and run via dual inlet on the IsoPrime mass spectrometer. All results are reported with respect to VPDB, normalised to an internal GNS Marble standard (2.04‰ for $\delta^{13}C$ and -6.40‰ for $\delta^{18}O$). Precision is 0.1‰ for $\delta^{13}C$ and 0.2‰ for $\delta^{18}O$ (Appendix, Supp. Information).

4.4 Organic geochemistry

A total of 68 samples were analysed for glycerol dialkyl glycerol tetraethers (GDGTs) at the Organic Geochemistry Unit, University of Bristol (Appendix, Supp. Information). Sediments were freeze-dried and powdered with a pestle and mortar. Biomarker lipids were extracted from between 30 and 50 g of sediment using Soxhlet technique and 220 ml of a 9:1 mixture (v/v) of dichloromethane (DCM) and methanol (MeOH). Sediments were extracted for 24 hrs at ~70 °C with activated copper to remove elemental sulfur. The total lipid extract (TLE) was concentrated using a rotary evaporator, then dried under a gentle flow of nitrogen. Open column flash chromatography (alumina) was used to separate the TLE into apolar and polar fractions using 4 ml of dichloromethane (DCM):hexane (9:1) and 4 ml of DCM:Methanol (MeOH) (1:2), respectively. Both fractions were fully dried under a gentle flow of nitrogen. The polar fraction was redissolved in a mixture of hexane and *iso*-propanol (IPA) (99:1) and filtered through a 0.45 μm PTFE filter. Filtered polar fractions were analysed for their core-lipid GDGTs distribution by high performance liquid chromatography/atmospheric pressure chemical ionisation-mass spectrometry (HPLC/APCI-MS) using a ThermoFisher Scientific Accela Quantum Access triplequadrupole MS. Normal phase separation was achieved using two ultra-high performance liquid chromatography silica columns, following the methods of Hopmans et al. (2016). Injection volume was 15 out of 100 μl. Analyses were performed using selective ion monitoring mode (SIM) to increase sensitivity and reproducibility (*m/z* 1302, 1300, 1298, 1296, 1294, 1292, 1050, 1048, 1046, 1036, 1034, 1032, 1022, 1020, 1018, 744, and 653). Sample results were integrated manually using the Xcalibur software.

4.5 GDGT-based calibrations and indices

We used the distribution of isoprenoidal GDGTs as reflected in the TetraEther indeX of tetraethers consisting of 86 carbon atoms (TEX$_{86}$) to reconstruct SST (Schouten et al., 2002).

$$\mathrm{eq.\,(1)\ TEX_{86}} = \frac{[iso\mathrm{GDGT\text{-}2}] + [iso\mathrm{GDGT\text{-}3}] + [cre.\,regio\ isomer]}{[iso\mathrm{GDGT\text{-}1}] + [iso\mathrm{GDGT\text{-}2}] + [iso\mathrm{GDGT\text{-}3}] + [cren.\,regio\ isomer]}$$

257 To capture the range of potential SST estimates that may be derived from this proxy we applied two

258 different calibrations: the BAYSPAR deep time analogue calibration (Tierney and Tingley, 2014,

259 2015; Tierney et al., 2017), which is based on a linear relationship between TEX_{86} and SST, and the

260 TEX_{86}^H calibration (Kim et al., 2010), which is based on an exponential relationship (Hollis et al.,

261 2019). The TEX_{86}^L calibration is not used because it has been found to have significant shortcomings

262 (Hollis et al., 2019). The BAYSPAR deep-time calibration has been applied to reconstruct SSTs

263 during greenhouse periods such as the early Paleogene (Naafs et al., 2018), PETM (Tierney and

264 Tingley, 2014) and Cretaceous (Naafs and Pancost, 2016; O'Brien et al., 2017). For the BAYSPAR

265 calibration, we used a prior of $30 \pm 20°C$ and search tolerance of 0.13. The resulting analogue

266 locations are all located in the tropics or subtropics, including the Red Sea (this data is excluded from

267 the TEX_{86}^H calibration). Selecting different values for the prior (e.g. 25–35°C) does not result in

268 significantly different SST results. Although part of our data lies above the modern calibration range

269 for TEX_{86}, the data lie within the range of mesocosm experiments that indicate TEX_{86} remains

270 (linearly) correlated to temperature at SSTs up to 40 °C (Schouten et al., 2007). The BAYSPAR deep-

271 time calibration incorporates this range into its error calculation.

272 Following Inglis et al. (2015) we identify an *iso*GDGT distribution similar to that found at

273 present in the Red Sea (Trommer et al., 2009) using;

274 $$eq. (2) \ isoGDGT_{rs}(\%) = \frac{[cren. regio \ isomer]}{[cren. regio \ isomer] + [isoGDGT\text{-}0]} \times 100$$

275 In addition, we also calculate the Branched versus Isoprenoidal Tetraether (BIT) index (Hopmans

276 et al., 2004).

277 $$eq. (3) \ BIT = \frac{Ia + IIa + IIa' + IIIa + IIIa'}{Ia + IIa + IIa' + IIIa + IIIa' + cren.}$$

278 BIT reflects the relative abundance of *br*GDGTs that are abundant in mineral soil and peat (Weijers et

279 al., 2006; Weijers et al., 2007; Naafs et al., 2017b) versus a specific archaeal *iso*GDGT, crenarchaeol,

280 produced by *Thaumarchaeota* that is more abundant in the marine realm (Sinninghe Damsté et al.,

281 2002). High BIT values are typically found in soils and lacustrine archives, and are therefore

282 generally used to indicate a high input of terrestrial-derived GDGTs, which can result in unreliable

283 SST estimates (Hopmans et al., 2004). However, it is important to note that brGDGTs can also be

284 produced *in situ* in marine sediments and do not always purely reflect changes in terrestrial input

285 (Sinninghe Damsté, 2016). BIT values <0.3 indicate terrestrial-derived GDGTs likely have little effect

286 on TEX_{86}-based SST estimates (Hopmans et al., 2004).

287 The methane index (MI) (Zhang et al., 2011) is defined as;

288 eq. (4) $MI = \dfrac{[isoGDGT\text{-}1] + [isoGDGT\text{-}2] + [isoGDGT\text{-}3]}{[isoGDGT\text{-}1] + [isoGDGT\text{-}2] + [isoGDGT\text{-}3] + [Cren.] + [cren.\,regio\,isomer]}$

289 A MI >0.5 indicates a contribution of methanogens to the GDGT pool that can bias TEX_{86}-based SST.

290

291 **5. Results**

292 *5.1 Stratigraphy, age control and fossil assemblages*

293 The stratigraphy of the section is described in relation to five Eocene New Zealand Stages

294 (Fig. 2): Waipawan, Mangaorapan, Heretaungan, Porangan and Bortonian (Cooper et al., 2004; Raine

295 et al., 2015), which extend from earliest Eocene to latest middle Eocene (56 to 39.1 Ma).

296 Biostratigraphic data are in the Appendix (Supp. Information).

297

298 *5.1.1. Lithostratigraphy*

299 The ~80 m section is mainly a moderately indurated, partly calcareous, grey mudstone, which

300 is glauconite rich in the upper part of the section. An abrupt coarsening of sediment occurs at ~59 m,

301 with overlying sediments containing common medium- to coarse-grained glauconite (Fig. 3).

302 Magnetostratigraphy and calcareous microfossil biostratigraphy provide a good age framework

303 (Dallanave et al., 2016). The section extends from lower–middle Eocene (~55.5–42 Ma; Waipawan–

304 lower Bortonian), with an unexposed interval in the Waipawan part of the section (-13.1 to -6.7 m).

305 The abrupt change in sediment type at 59 m coincides with an unconformity that spans ~3 Myr:

306   uppermost Heretaungan, Porangan and lowermost Bortonian (middle Eocene) sediments are not

307   preserved.

308

309   *5.1.2 Foraminifera*

310   Foraminifera are poorly preserved in the lowermost part of the section (-16.15 to -13.2 m),

311   but an earliest Eocene (Waipawan) age is inferred from identifiable specimens of *Globanomalina*

312   *australiformis* and *Morozovella aequa* (Fig. 3). Foraminifera are relatively well preserved, abundant

313   and diverse above the unexposed section, from -6.61 to 66.5 m, although preservation is poor above

314   59 m, coincident with the occurrence of greensand beds. The Waipawan/Mangaorapan boundary is

315   identified at -3.99 m based on the lowest occurrence (LO) of *Morozovella crater*. The base of the

316   Heretaungan stage is identified by the LO of the marker benthic species *Elphidium hampdenense* at

317   27.51 m, and the species is present up to 58.55 m. Two species of the genus *Morozovella*, *M. crater*

318   and *M. lensiformis*, are present in all samples from -3.99 to 57.9 m and the genus is only absent in the

319   uppermost Heretaungan sample (58.55 m). The primary datum for the Porangan Stage, benthic

320   species *Elphidium saginatum*, is not identified in the section. The base of the Bortonian is identified

321   by the primary datum, LO of *Globigerinatheka index*, directly above the unconformity at 59.71 m,

322   and is supported by the LOs *of Bulimina bortonica* at 59.71 m and *Acarinina primitiva* at 63.05 m.

323   Planktic foraminiferal abundance is low in the early Waipawan (average 3%) but increases to

324   >40% in the late Waipawan. Several pulses of high abundance, >70%, are seen in the early–middle

325   Mangaorapan, whereas the late Mangaorapan has stable planktic abundance (Fig. 3). There is a

326   general abundance drop in the Heretaungan, with the average value (38%) noticeably lower than in

327   the Mangaorapan (65%).

328

329   *5.1.3 Calcareous nannofossils*

330   A summary of the detailed calcareous nannofossil biostratigraphy by Shepherd and Kulhanek

331   (2016) is provided here. The presence of *Rhomboaster bramlettei* at -15.25 m places base of the

section in Zone NP10, early Eocene (Fig. 3). The LO of *Sphenolithus radians* at -6.61 m is used as a secondary marker for the base of NP11 (Backman, 1986) rather than the index species *Tribrachiatus contortus*, which is absent. The LO of *Tribrachiatus orthostylu*s, an event within the upper part of NP10 (Pälike et al., 2010), co-occurs with the LO of *S. radians*, suggesting the upper part of NP10 is within the non-exposed interval from -13.2 to -6.6 m. The LO of *Discoaster lodoensis* at -2.87 m, earliest Mangaorapan, marks the base of NP12. It is possible that *D. lodoensis* has a delayed LO at mid-Waipara, given that in the nearby Mead Stream section the LO of *D. lodoensis* occurs ~36 m below the LO of *Morozovella crater* and at mid-Waipara these two bioevents occur within ~1 m (Supp. Information Fig. 2). The HO of *T. orthostylus*, marker for the base of NP13, is observed at 11.13 m and lower Chron C22r (mid-Mangaorapan). The absence of *Discoaster sublodoensis*, marker for the base of NP14, means the NP13/NP14 boundary cannot be identified. However, the base of NP14 is known to occur in lower Chron C22n (Hollis et al., 2019), which is well-defined at mid-Waipara. From this we infer that the NP13/14 boundary lies in the late Mangaorapan, between ~20.7 and 27 m. Some or all of Zone NP15 (i.e., late Heretaungan–latest Porangan) is inferred to be missing because the markers for the base of NP15 and base of Subzone NP15b (LOs of *Nannotetrina fulgens* and *Chiasmolithus gigas*, respectively) are not observed. The base of NP16 is difficult to identify as both the primary and secondary markers, *Blackites gladius* and *Nannotetrina alata/fulgens*, are not observed. However, *Reticulofenestra umbilicus* (>14μm) and *Reticulofenestra reticulata* both have LOs in Zone NP16 (Pälike et al., 2010) and at mid-Waipara they co-occur at 62.26 m, early Bortonian. This suggests the lower part of Zone NP16 is missing, given that *R. reticulata* evolved at least several hundred thousand years after *R. umbilicus* (Gradstein et al., 2012; Agnini et al., 2014). Nannofossil and foraminiferal biostratigraphy agree that the unconformity at ~59 m encompasses the latest Heretaungan–earliest Bortonian (Fig. 3).

       Nannofossil preservation is linked to carbonate content in this section. A positive correlation is observed between carbonate content and the visual observation of preservation (VOP), as well as the relative abundance of *Zygrhablithus bijugatus*, a species sensitive to dissolution (Jiang and Wise, 2009; Fig. 4). Poorly preserved assemblages occur in the Waipawan (NP10) and upper Heretaungan

359 (NP14) parts of the section where $CaCO_3$ is <10% and generally <15%, respectively. The best-

360 preserved assemblages are in the Mangaorapan, from the base of Zone NP12 to NP13–lower NP14,

361 where $CaCO_3$ is >15%. An increase in taxon richness and diversity is seen from the base of NP12,

362 consistent with the increase in preservation. Overall, the covariance between preservation and

363 diversity indices suggests preservation is an important factor influencing diversity in this section

364 (Shepherd, 2017).

365

366 *5.1.4 Dinoflagellate cysts*

367 Dinocyst assemblages are generally abundant and well preserved. Integration of index taxa

368 (Wilson, 1988; Morgans et al., 2004) with magnetostratigraphy and calcareous microfossil

369 biostratigraphy allows the age control of key species to be improved (Fig. 3). In the Waipawan, the

370 LOs of several zonal taxa are recorded: *Samlandia delicata* (NZE2a, -15.25 m) and *Impagidinium*

371 *cassiculum* (NZE2b, -13.20 m) occur in nannofossil Zone NP10, whereas the LO of *Dracodinium*

372 *waipawaense* (NZE3) is in Zone NP11 (-6.61 m). The range of *Wilsonidium ornatum* (NZE4) is

373 restricted to the Mangaorapan (Zone NP12 to NP13; -2.87–17.83 m). The LOs of key taxa

374 *Charlesdowniea coleothrypta* (19.98 m) and *Charlesdowniea edwardsii* (22.14 m) occur in the late

375 Mangaorapan. The HO of *C. coleothrypta* (26.75 m) is in upper Chron C22n, close to the

376 Mangaorapan/Heretaungan boundary, and the HO of *C. edwardsii* is early Heretaungan (32.40 m).

377 The onset of common–frequent *Membranophoridium perforatum*, a regional bioevent (Wilson, 1984,

378 1988), occurs in the Heretaungan close to the Chron C21r/C21n boundary.

379 Additional taxa offer potential to further refine the early–middle Eocene zonation. The LO of

380 *Impagidinium crassimuratum* and HO of *Manumiella rotunda* occur in Zone NP10 (early Waipawan).

381 The LOs of *Membranophoridium perforatum*, *Schematophora obscura* and the genus *Homotryblium*

382 are in Zone NP11 (late Waipawan). The LO of *Danea crassimuratum* is in Zone NP12 (early

383 Mangaorapan). The LO of *Achilleodinium biformoides*, *Deflandrea antarctica* and *Impagidinium*

384 *parvireticulum* are in Chron C22n (late Mangaorapan). The HO of the *Apectodinium* genus is close to

385 the Chron C22r/C22n boundary, late Mangaorapan. Fewer bioevents are seen in the Heretaungan.

386   Endemic Antarctic Community taxa (Bijl et al., 2011), *Alterbidinium assymetricum* and *Spinidinium*

387   *macmurdoense*, have LOs in lower Chron C21r, correlated with Zone NP14.

388

389   *5.1.5 Spores and pollen*

390   Spore and pollen abundance ranges from 22–43% of the total palynomorph assemblage.

391   Three zones (Raine, 1984; Morgans et al., 2004) are identified: PM3b, MH1 and MH2 (Fig. 3). The

392   lower part of the section (-16.15 m to -13.2 m) is correlated with the earliest Eocene PM3b Zone,

393   based on thermophilic taxa *Cupanieidites orthoteichus* and *Spinizonocolpites prominatus*, and rare

394   *Myricipites harrisii* (Raine et al., 2009; Handley et al., 2011). The base of Zone MH1, defined by a

395   noticeable increase in *M. harrisii* abundance, occurs between -13.2 m and -6.61 m (late Waipawan).

396   *M. harrisii* is common–abundant from this level to the late Heretaungan (57.93 m) and this interval is

397   correlated with Zone MH1. The tropical-subtropical spore *Crassoretitriletes vanraadshooveni*

398   (*Lygodium*) has a HO in the late Mangaorapan. The overlying Bortonian interval is correlated with

399   Zone MH2 based on the presence of *Nothofagidites flemingii*.

400

401   *5.2 Carbonate content, and carbon and oxygen isotopes*

402   Carbonate ($CaCO_3$) content is relatively low in the mid-Waipara section, never >30% (Fig.

403   5a). It is <15% in the earliest Eocene (early Waipawan) and most of the middle Eocene

404   (Heretaungan–early Bortonian). The highest $CaCO_3$ values, albeit variable, are in the late Waipawan

405   and Mangaorapan (early Eocene), also where well-preserved and abundant calcareous microfossil

406   assemblages are recovered. The primary source for $CaCO_3$ in this section is assumed to be calcareous

407   nannofossils. Variation in the relative abundance of planktic foraminifera suggests that the secondary

408   source may vary from calcareous benthic foraminifera in the early Waipawan and Heretaungan–

409   Bortonian, to planktics in the Mangaorapan. $CaCO_3$ content has a weak negative correlation with bulk

410   carbonate $\delta^{13}C$ (r = -0.25, n = 68, *p* <0.05), is not correlated with $\delta^{18}O$, and has a strong positive

411   correlation with TEX_{86} (r = 0.60, n = 68, *p* <0.001). Under typical ocean conditions, benthic

412 foraminifera will have lower $\delta^{13}C$ values than planktic foraminifera because the biological carbon

413 pump delivers ^{12}C-enriched organic matter to the sea floor.

414 Bulk carbonate $\delta^{13}C$ values range from -0.8‰ to 1.6‰, with a general trend towards higher

415 values from early to middle Eocene (Fig. 5b). A positive excursion, of ~1‰, occurs in the earliest

416 Eocene (early Waipawan). The most negative $\delta^{13}C$ value in the section, -0.8‰, is recorded at -6.61 m

417 in the late Waipawan, Zone NP11, and marks the first of a series of six (#1–6) negative carbon isotope

418 excursions (CIEs) in the Waipawan–Mangaorapan (early Eocene), which are superimposed on a

419 positive $\delta^{13}C$ trend. The $\delta^{13}C$ minimum within each CIE also increases over time, from -0.7‰ at -2.12

420 m to 0.7‰ at 26.75 m. A baseline positive shift (0.7–1.5‰) is recorded across the

421 Mangaorapan/Heretaungan boundary. Through most of the Heretaungan $\delta^{13}C$ values remain stable,

422 although a shift to lower values occurs in the late Heretaungan between ~50 and 59 m. The Bortonian

423 section is marked by variable $\delta^{13}C$ values, from -0.2‰ to 1.4‰, with a possible negative CIE at 62.26

424 m. The CIEs tend to be associated with lower $CaCO_3$ values but not in all cases (e.g., CIEs #3 and

425 #5). Some of the negative shifts in $\delta^{13}C$ in the earliest Waipawan and Heretaungan may be partly due

426 the low abundance of planktic foraminifera, because benthic foraminiferal calcite is generally more

427 enriched in ^{12}C. However, the lack of a consistent relationship between the CIEs in the late Waipawan

428 and Mangaorapan and planktic abundance suggests that foraminiferal calcite is not the primary source

429 of carbonate in this interval.

430 The bulk carbonate $\delta^{18}O$ record is not correlated with other geochemical proxies (Appendix,

431 Supp. Information Fig. 3) and the general trend is inconsistent with other early Eocene $\delta^{18}O$ records

432 (e.g., Westerhold et al., 2018; Barnet et al., 2019). Values in the range of -2.5 to -4‰ yield

433 temperatures in the range of 22–30°C, which are consistent with SSTs reported in previous studies

434 (Hollis et al., 2009, 2012). However, these values are interspersed with $\delta^{18}O$ values that range from -4

435 to -6.4‰ and yield unrealistically hot temperatures (up to 42°C). These values are likely to result

436 from post-depositional interactions with ^{18}O-depleted meteoric water (Hollis et al., 2012). Because we

437 have no way of discriminating between reliable and unreliable values, the bulk oxygen $\delta^{18}O$ record is

438   not discussed further in this article. The bulk carbonate $\delta^{13}C$ record is not affected by meteoric water

439   interactions.

440

441   *5.3 GDGT distributions*

442   Both isoprenoidal and branched GDGTs are present in all samples, and the TEX_{86} and BIT

443   records are broadly consistent with previously reported Eocene records from this section (Hollis et al.,

444   2009, 2012). The most notable change in the TEX_{86} record is in the basal part of the section, where

445   values increase from 0.65–0.7 in the early Waipawan to >0.8 in the late Waipawan (Fig. 5c). These

446   high TEX_{86} values continue up to 5.23 m in the early Mangaorapan (Chron C23n.2n). The overlying

447   TEX_{86} record is characterized by a gradual decline into the middle Eocene, with a sharp decrease at

448   the Mangaorapan/Heretaungan boundary. Average TEX_{86} values in the Heretaungan are lower (0.7)

449   than in the Mangaorapan (0.8). TEX_{86} values in the early Bortonian, Zone NP 16, are variable and

450   range between 0.55 and 0.7. There is a strong negative correlation (r = -0.54, n = 68, p <0.001)

451   between TEX_{86} and bulk carbonate $\delta^{13}C$. Most early Eocene CIEs appear to be associated with higher

452   TEX_{86}, implying that these CIEs represent hyperthermals.

453   The methane index (MI) is ≤ 0.30 in all samples, indicating that TEX_{86} values are not biased

454   by a large contribution of methanogens to the GDGT pool. Low BIT indices (<0.25) throughout the

455   section indicate that TEX_{86} values are likely not significantly biased by terrestrial input. BIT values

456   are lowest (<0.1) in the Waipawan and increase progressively through the overlying Mangaorapan

457   and Heretaungan Stages (Fig. 5d). The BIT index is highly variable in the early–middle Mangaorapan

458   (Zone NP12), with lower values associated with the hyperthermals (high TEX_{86}) and higher values

459   associated with positive excursions in bulk carbonate $\delta^{13}C$. Overall, the BIT index exhibits a weak

460   negative correlation with TEX_{86} and a strong positive correlation with $\delta^{13}C$ (r = -0.24, p <0.05 and

461   0.65, p <0.001, respectively, n = 68). The anticorrelation between the BIT index and $\delta^{13}C$ is difficult

462   to interpret, if we assume the BIT index purely reflects changes in terrestrial input, particularly the

463   decrease in BIT and, hence, terrigenous supply during the negative CIEs. Previous studies in Eocene

464   sections to the north (Marlborough, Fig. 1) have shown that hyperthermals are associated with

465   increased terrigenous input in bathyal settings (Hollis et al., 2005a; Nicolo et al., 2007; Slotnick et al.,

466   2012, 2015), and this would be expected to be associated with an increase in BIT values. At mid-

467   Waipara, however, we observe a decrease in BIT values during negative CIEs, which implies reduced

468   terrigenous input and may be a localised response to transient climate events, such as current

469   winnowing of finer sediments. However, the BIT index can be influenced by other factors and does

470   not always purely represent a simple two end-member model between pure marine and terrestrial

471   input. For example, the reduced BIT could reflect a relative increase in crenarchaeol over brGDGT

472   input during the hyperthermals, or the BIT may respond to changes in the contribution of *in situ*

473   produced brGDGTs to the sedimentary GDGT pool. Either way, the low BIT values indicate that a

474   relatively low amount of the GDGT pool is derived from soils.

475   The brGDGTs found in these marine samples (Appendix) could also contain brGDGTs

476   generated in the water column or marine sediments, rather than from land-based soils, which

477   complicates the use of brGDGTs in these sediments to quantify terrestrial temperature (De Jonge et

478   al., 2014b; Sinninghe Damsté, 2016). A non-soil source of brGDGTs to the sediments at mid-Waipara

479   is further supported by the observation that the relative abundance (%) of penta- or hexamethylated

480   versus tetramethylated brGDGTs is higher than that seen in any modern mineral soil or peat (Supp.

481   Information Fig. 4). The number of rings of pentamethylated brGDGTs versus the number of rings of

482   hexamethylated brGDGTs is also significantly higher than that seen in any modern mineral soil or

483   peat. We therefore do not discuss brGDGT-based terrestrial temperatures at mid-Waipara River.

484

485   *5.4 The Early Eocene Climatic Optimum in the mid-Waipara River section*

486   A combination of biostratigraphy, magnetostratigraphy, bulk carbonate $\delta^{13}C$ values and

487   TEX$_{86}$ is used to determine the position of the EECO in the mid-Waipara section. As discussed

488   earlier, the EECO is inferred to extend from 53.26–49.14 Ma, Chron C24n.2r (J event, mid-NP11) to

489   uppermost Chron C22n (C22nH5 event, lower NP14) (Westerhold et al., 2018). The lowest chron

490   identified in mid-Waipara is C23.2n, which lies in Zone NP12 (Fig. 5). The interval directly overlying

491   the unexposed interval in the lower part of the section (Waipawan, -6.61 m) is correlated with NP11,

492   has the highest TEX_{86} values in the section, and also has what we infer to be the first of six CIEs in

493   the section. For these reasons, we place the base of the EECO at this level (Fig. 6). There are

494   uncertainties, however, constraining the age of the lower part of the section (Supp. Information Fig.

495   2), and we infer the CIE at this level (#1) to correspond with either the J event (C24n.2rH1) or the K

496   event (C24n.1nH1). The upper limit of the EECO in this section is well recorded. We place it at the

497   uppermost CIE (#6), which lies within upper Chron C22n and coincides with the onset of a cooling

498   trend in the TEX_{86} record (Fig. 5). Given the age of the Mangaorapan/Heretaungan boundary, at 49.27

499   Ma (C22n(0.6)) and magnetostratigraphy in this part of the section, we infer CIE #6 to correspond

500   with the C22nH4 event (49.25 Ma). This suggests that cooling at mid-Waipara began slightly earlier

501   than the top EECO as recognised by Westerhold et al. (2018) at 49.14 Ma (C22nH5).

502   Combining these two datums with the integrated magnetobiochronology for the section

503   (Appendix, Supp. Information), calibrated to the timescale of Westerhold et al. (2017), allows us to

504   provisionally correlate the other CIEs in the section as follows: #2 = C23rH2 or M event; #3 =

505   C23n.2nH2 or O event; #4 = C22rH1 or Q event; #5 = C22rH4 or T event (Fig. 6). The major positive

506   shift in $\delta^{13}C$ during C23n (51.2–51 Ma; Westerhold et al., 2018) is not clearly observed at mid-

507   Waipara, perhaps due to the presence of cryptic unconformities in this part of the section.

508

509   *5.5 Paleoenvironmental changes*

510   *5.5.1 Foraminiferal assemblage*

511   Benthic foraminiferal paleodepth indicators (e.g. *Pleurostomella*, *Stilostomella* and

512   *Bathysiphon* spp.) suggest that the entire section was deposited in a middle bathyal setting (Appendix,

513   Supp. Information). The incoming of *Nuttallides carinotrumpyi* and the genera *Karreriella* and

514   *Vulvulina* in the early EECO (late Waipawan and early Mangaorapan) indicate a deeper bathyal

515   setting. The presence of *Tritaxilina zealandica*, from mid EECO to earliest post-EECO (middle

516   Mangaorapan–early Heretaungan), suggests that this is the deepest interval in the section, probably

517   lower bathyal (Hayward, 1986; Hayward et al., 2010). Foraminiferal assemblages higher in the post-

518   EECO Heretaungan indicate shallowing with the disappearance of *Karreriella* and *T. zealandica*,

519   although middle bathyal indicators persist into the Bortonian.

520   Foraminiferal assemblages are affected by preservation. The best-preserved assemblages are

521   in the late Waipawan–Mangaorapan (EECO) where $CaCO_3$ content is highest. Planktic abundance

522   (Fig. 3) is also correlated with carbonate content ($CaCO_3$, r = 0.76, n = 26, *p* <0.001) although this

523   may be due to a combination of factors, such as improved preservation and warmer conditions. Peaks

524   in planktic abundance align with three of the negative CIEs (#1, 2, 5) and may be directly related to

525   warmer SST or indirectly linked to warming by increased clay content, which can enhance

526   preservation (Hollis et al., 2019). However, we have not confirmed that CIEs in this section are

527   accompanied by an increase in clay. A strong correlation with TEX_{86} (r = 0.84, n = 26, *p* <0.001)

528   provides further evidence that planktic abundance is linked to temperature. In the early Waipawan

529   (below the EECO), a combination of cooler SST (Fig. 5c) and poor preservation perhaps led to low

530   planktic abundance, despite the middle bathyal depositional setting. A similar trend is evident in the

531   late Heretaungan.

532

533   *5.5.2 Dinocyst assemblage*

534   Gonyaulacoid dinocysts, representative of autotrophic dinoflagellates (Dale, 1996), dominate

535   the Eocene assemblages and include the genera *Spiniferites*, *Operculodinium*, *Cerebrocysta* and

536   *Impagidinium* (Fig. 7). Peridinioids (e.g., *Spinidinium* spp.), predominantly heterotrophic

537   dinoflagellates, comprise <30% of the assemblage, apart from an interval in the late EECO (late

538   Mangaorapan) where they become super-abundant. Assemblages below the EECO, early Waipawan,

539   are dominated by cosmopolitan taxa, such as *Elytrocysta* spp., *Operculodinium* spp. and *Spiniferites*

540   spp., and peridinioids are frequent. Compared with the early Waipawan, assemblages in the EECO

541   (late Waipawan–Mangaorapan) are more diverse, with new taxa (e.g., *Batiacasphaera* spp.,

542   *Membranophoridium perforatum*, *Schematophora obscura*) becoming common, some cosmopolitan

543   taxa (e.g., *Elytrocysta* spp., *Operculodinium* spp.) declining in abundance, and taxa such as *Diphyes*

544   spp., *Hystrichokolpoma* spp. and *Impagidinium cassiculum* increasing in abundance. The tropical–

warm temperate genus *Homotryblium* is frequent–abundant in the early and middle EECO, with three main abundance peaks ranging from 19–30%. In the late EECO, there is a significant increase (up to 40%) in peridinioid abundance, and they continue to be frequent–abundant in the overlying post-EECO Heretaungan. Early Bortonian samples are a mix of cosmopolitan and more endemic (e.g., *Enneadocysta*) taxa.

5.5.3 Spore and pollen assemblage

Spores and pollen average 37% of palynomorph assemblages below the EECO (Fig. 8). This abundance declines in the early–middle EECO, with a minimum value of 22% in Chron C22r, begins to increase in the late EECO, and increases slightly in the post-EECO Heretaungan. Spore and pollen abundance has a strong negative correlation (r = -0.61, n = 35, p <0.001) with TEX$_{86}$ and a moderate positive correlation (r = 0.33, n = 35, p <0.05) with BIT index. The parallel trend of increasing terrestrial palynomorphs and BIT index in the late EECO and post-EECO Heretaungan suggests an increasing contribution of terrestrial material in the sedimentary record as temperatures cooled following the peak-EECO warmth.

Pre-EECO assemblages are dominated by gymnosperm pollen (up to 71%), particularly *Podocarpidites* and the Araucarian taxon *Dilwynites granulatus*, and *Cyathidites* fern spores (Fig. 8). In contrast, the early EECO shows a marked increase in angiosperm pollen, from <15% in the early Waipawan up to 44% in the early Mangaorapan, and a concomitant decline in gymnosperm abundance, most notably *Podocarpidites*. This angiosperm increase is mainly driven by a rise in Casuarinaceae (*Myricipites harrisii*), although other angiosperms become more common, including *Malvacipollis subtilis*, *Proteacidites* and *Tricolporopollenites latizonatus*. Vegetation remains relatively stable in the EECO, with only a minor increase in *D. granulatus* and *Podocarpidites* gymnosperms in the late EECO. The abundance of *M. harrisii*, and total angiosperms, decline slightly in the Heretaungan and continue to decline in the early Bortonian, along with the incoming of the cooler southern beech family Nothofagaceae genus *Nothofagus* (*Nothofagidites flemingii*).

5.6 Microfossil paleotemperature indicators

The relationship between microfossil assemblages and latitudinally constrained environmental parameters, such as temperature and salinity, has been widely used to define biogeographic zones, both in the modern ocean (e.g., McIntyre and Bé, 1967; Okada and Honjo, 1973; Prebble et al., 2013; Zonneveld et al., 2013) and in the geological record (e.g. Haq, 1981; Hennissen et al., 2017). Whilst many environmental parameters have the potential to influence microfossil distribution, SST has been shown to be the most important variable for calcareous nannofossil (e.g., Haq et al., 1977; Haq, 1981; Wei and Wise, 1990) and dinocyst assemblages (e.g., De Vernal et al., 2005; Sluijs et al., 2005; Prebble et al., 2016; Frieling and Sluijs, 2018).

Warm-water indicators in the calcareous nannofossil assemblage, namely *Discoaster* spp., *Sphenolithus* spp. and *Coccolithus formosus*, are most abundant in the early and middle EECO, with a combined abundance up to 19% (Fig. 4). The combined abundance of this warm-water group is also high in the early Waipawan, below the EECO, and in the latest Heretaungan, post-EECO. This, however, is due to the high preservation potential of *Discoaster* spp., which dominates the warm-water assemblage in these intervals. In the EECO, cool-water indicators comprise <8% of the assemblage, and they become more abundant (up to 17%) in the post-EECO Heretaungan. Initially, the increase in cool-water taxa is related to an increase in *Reticulofenestra daviesii*, which is followed by an increase in *Chiasmolithus* spp. in the late Heretaungan. The cool-water group has a moderate negative correlation (r = -0.43, n = 30, *p* <0.02) with TEX$_{86}$, whereas the warm-water group has a weak positive correlation (r = 0.30, n = 30, *p* <0.1); the weaker correlation is likely due to the preservational effects noted above.

The abundance and diversity of the warm-water Wetzelielloideae dinocyst group is highest in the EECO, comprising up to 7% of the assemblage and 7 taxa, and the group disappears entirely in the post-EECO (Fig. 7). The warm temperate–tropical genus *Homotryblium* is first seen in the earliest EECO and is abundant (up to 30%) in the early and middle EECO, and generally lower in the post-EECO. The warm-water Wetzelielloideae group has a strong positive correlation (r = 0.59, n = 41, *p*

598 <0.001) with TEX_{86}, and there is a weak positive correlation (r = 0.29, n = 41, *p* <0.1) between

599 *Homotryblium* and TEX_{86}. Taxa of the Endemic Antarctic Community (EAC) group are first noted in

600 the late EECO, with abundance progressively increasing (up to 17%) in the post-EECO. The EAC

601 group has a strong negative correlation (r = -0.56, n =41, *p* <0.001) with TEX_{86}. These correlations

602 between calcareous nannoplankton and dinocyst fossil assemblage-based proxies for temperature and

603 the independent SST proxy, TEX_{86}, provide convincing evidence that both approaches are reliable

604 guides to past water temperature.

605   The main vegetation change is an increase in angiosperm pollen, driven by a rise in

606 Casuarinaceae (*Myricipites harrisii*) in the early EECO (Fig. 8). *M. harrisii* abundance has a strong

607 positive correlation with TEX_{86} (r = 0.76, n = 33, *p* <0.001). Angiosperms with affinities to

608 mesothermal–megathermal climates, such as *Anacolosidites*, *Bluffopollis scabratus*,

609 *Intratriporopollenites notabilis* and *Margocolporites cribellatus*, are rare but occur below, in, and

610 above the EECO (Appendix, Supp. Information). Most of these taxa do not occur in the cooler early

611 Bortonian, but the thermophilic *Spinizonocolpites prominatus* (*Nypa* mangrove) and *Malvacipollis*

612 *subtilis* taxa continue to be present.

613

614 *5.7 Sea-surface temperature*

615   While the evidence above, as well as numerous other multiproxy studies, show that TEX_{86} is

616 a robust guide to relative changes in SST (e.g., Zachos et al., 2005; Pearson et al. 2007), there is

617 ongoing debate about how the proxy relates to absolute temperature in the Paleogene, and especially

618 to mean annual SST in middle–high latitudes (Hollis et al., 2012). Here we use the two most widely

619 used calibrations, TEX_{86}^{H} (Kim et al., 2010) and $BAYSPAR_{SST}$ (Tierney and Tingley, 2015), which

620 yield similar absolute values in this record (Fig. 9a). TEX_{86}^{H} is based on an exponential relationship

621 with SST whereas BAYSPAR assumes a linear relationship, which results in higher values at the

622 upper end of the calibration (i.e. where TEX_{86} > 0.7) and especially beyond the range of the modern

623 calibration dataset. In our record, the amplitude of SST change is larger in $BAYSPAR_{SST}$ than in

624 TEX_{86}^{H} (Fig. 9b).

625   The most marked shift in SST is in the Waipawan, from pre-EECO to early EECO, with an

626   increase of between ~7 and 12°C (Fig. 9b). BAYSPAR SST increases from ~22.5 to 35.5°C, whereas

627   TEX_{86}^H SST increases from ~26 to 33.5°C. SST is highest in the early EECO and declines slightly

628   through the middle and late EECO. The baseline shift to a lower SST in Chron C23n.2n (~5.2 m),

629   corresponding with the C23n.2nH2 or O Event (Fig. 6), matches North Pacific records that indicate

630   the end of the warmest interval in the EECO occurs in uppermost Chron C23n.2n at 51.23 Ma

631   (Westerhold et al., 2018). A decrease in TEX_{86}-derived SST occurs across the

632   Mangaorapan/Heretaungan boundary, and SST continues to decline in the post-EECO Heretaungan.

633   Lower SST is present in the early Bortonian (middle Eocene, Zone NP16), although a transient peak,

634   up to 25.2°C ($BAYSPAR_{SST}$) and 27.9°C (TEX_{86}^H), is recorded and may represent the Middle Eocene

635   Climatic Optimum (MECO) at ~40 Ma.

636

637   *5.8 Red Sea-type GDGT distributions*

638   The $\%GDGT_{RS}$ distribution is used to identify sediments with unusually low amounts of

639   GDGT-0 relative to crenarchaeol regioisomer, which is characteristic for the GDGT distribution

640   found in modern sediments from the Red Sea (Trommer et al., 2009). Where $\%GDGT_{RS}$ >30 it is

641   inferred that the distribution is similar to that found in the Red Sea and may have added a warm bias

642   to SST estimates (Inglis et al., 2015). $\%GDGT_{RS}$ values >30 are common during times of elevated

643   warmth but may be a response to factors other than temperature given the distinct Red Sea archaeal

644   assemblages (Trommer et al., 2009). Crucially, the modern Red Sea data exert a particularly strong

645   influence on the high temperature end of all TEX_{86}-SST calibrations, depending on how they are

646   included (Inglis et al., 2015). At mid-Waipara River, $\%GDGT_{RS}$ values >30 are consistently observed

647   in the EECO, with the highest values in the early and middle EECO (Fig. 9c). $\%GDGT_{RS}$ values drop

648   to <30 across the Mangaorapan/Heretaungan boundary. $\%GDGT_{RS}$ values are <30 in the early

649   Waipawan (pre-EECO), Heretaungan (post-EECO) and early Bortonian.

650

6. Discussion

6.1 Comparison of proxy-based SST and microfossil records in the early and middle Eocene

Many early Paleogene studies have attempted to integrate climate proxy data with climate model simulations to understand global climate and carbon cycle response to elevated temperatures and greenhouse gases. While progress has been made in reconciling proxy temperature reconstructions with climate model simulations (Carlson and Caballero, 2017; Naafs et al., 2018), there remain known problems and inconsistencies with geochemical-based temperature proxies (Hollis et al., 2012, 2019). Multiproxy SST reconstructions (Mg/Ca ratios and $\delta^{18}O$ values of foraminiferal tests and GDGT-based TEX_{86} values) have been completed for the early–middle Eocene at mid-Waipara (Hollis et al., 2009, 2012; Inglis et al., 2015). The new TEX_{86}-based SST record presented here validates and complements these previous reconstructions (Fig. 10). The absolute SST values, however, remain debatable because they imply a reduced latitudinal temperature gradient between middle and low latitudes in the EECO and into the post-EECO, compared to the present (Cramwinckel et al., 2018; Naafs et al., 2018). In this context, the particularly warm temperatures (>30°C) in the Southwest Pacific warrant further investigation. Microfossil assemblages offer a means to explore these geochemical-based SST proxies and assess the faunal/floral evidence for tropical SSTs during the EECO in mid-latitudes (paleolatitude ~46°S) of the Southwest Pacific. We have found a good correlation between the trends in the TEX_{86} SST proxy and water temperature indicators within calcareous nannofossil and dinocyst assemblages.

Comparison of early–middle Eocene nannofossil assemblages from mid-Waipara with coeval records from subtropical (Shatsky Rise), temperate (Exmouth Plateau and Campbell Plateau) and subpolar (Kerguelen Plateau) provinces indicate that mid-Waipara assemblages are most similar to the other temperate sites, rather than assemblages at the subtropical setting (Fig. 11). Warm-water taxa (*Coccolithus formosus*, *Discoaster* spp., *Sphenolithus* spp.) are most abundant in the EECO at mid-Waipara, reaching up to 19% of the total assemblage. This is comparable with Site 762 (paleolatitude ~38°S), Exmouth Plateau, where warm-water taxa comprise up to 24% in the EECO (Schneider et al., 2011), and Site 277 (paleolatitude ~54°S), Campbell Plateau (Shepherd, 2017). Warm-water taxa at

678 the subtropical Site 1210 (paleolatitude ~28°N), Shatsky Rise, comprise up to 49% in the EECO

679 (Schneider et al., 2011). Indeed, there is a three-fold increase in the abundance of warm-water taxa in

680 the EECO between mid-Waipara (average 11%) and Site 1210 (average 35%). Conversely, cool-water

681 taxa (*Chiasmolithus* and *Reticulofenestra* spp.) are notably more abundant in the EECO, up to 18%, at

682 the polar Site 1135 (paleolatitude ~59°S), Kerguelen Plateau (Schneider et al., 2011), compared to

683 <10% at mid-Waipara, Campbell Plateau and Exmouth Plateau temperate sites. Cool-water taxa do

684 not significantly increase in abundance at mid-Waipara and Site 277 until after the EECO (Fig. 11).

685   Dinocyst assemblages at mid-Waipara exhibit a trend that is comparable to nannofossil

686 observations. The abundance and diversity of the warm-water Wetzelielloideae group is highest in the

687 EECO but the group comprises only a minor component (<10%) of the total assemblage (Fig. 12e). It

688 is estimated the lower SST tolerance of Wetzelielloideae was 20 ± 2.5°C (Frieling et al., 2014,

689 Frieling and Sluijs, 2018). Representatives of the Wetzelielloideae group are present below the EECO

690 and the group disappears above the EECO; however, TEX_{86}-based SST is well above 20°C in this

691 Waipawan–Heretaungan interval (Fig. 12b). This suggests that the disappearance of the group may be

692 linked to other factors in addition to cooling, such as changes in nutrients or fresh-water input. The

693 warm temperate–tropical genus *Homotryblium* peaks in abundance, up to 30%, in the lower–middle

694 EECO. The continued presence of *Homotryblium* above the EECO and in the early Bortonian

695 indicates a tolerance to a broader SST range than the Wetzelielloideae group, in contrast to

696 suggestions it preferred SSTs >25°C (Frieling and Sluijs, 2018), or perhaps an evolutionary

697 adaptation to post-EECO cooling (e.g., Dybkjær, 2004). The high *Homotryblium* abundance in the

698 EECO may be due to a combination of high SST and specific surface-water conditions (see section

699 6.3). The cooler-water EAC group first appear at mid-Waipara in the late EECO and, as with

700 nannofossils, become more common in the post-EECO (Fig. 12d, e). The increase in these cooler-

701 water groups suggests that the temperature gradient between the middle and low latitudes was

702 increasing in the post-EECO middle Eocene, perhaps related to tectonic processes such as the

703 deepening of the Tasmanian Gateway (Bijl et al., 2013b; Sijp et al., 2016).

704   Calcareous and organic marine microfossils from mid-Waipara show that elements of low-

705   latitude provinces existed in the early Eocene in the New Zealand region and became more diverse

706   and abundant in the EECO, but that marine assemblages characteristic of low-latitude Eocene oceans

707   were by no means dominant in the extended period of early Eocene warmth. In fact, nannofossil

708   assemblages indicate that temperature gradients between mid- and low-latitudes in the EECO were

709   greater than indicated by geochemical SST proxies. In the EECO, there are three times as many

710   warm-water indicators in the nannofossil assemblage at the low-latitude Shatsky Rise site (average

711   35%) as there are at the mid-latitude mid-Waipara section (average 11%). This is in contrast with

712   geochemical-based SST proxies, where average SSTs in the EECO only differ by 5°C across the same

713   latitudinal range and climate zones.

714   Despite these apparent discrepancies between absolute temperature inferred from

715   geochemical proxies and fossil biogeography, microfossil assemblages and SST proxies are in good

716   agreement in the trend of relative temperature change in the early–middle Eocene. TEX$_{86}$-based

717   records indicate pronounced warming of between ~7 and 12°C (Fig. 9) from pre-EECO to early

718   EECO. This is also associated with the most notable biotic change in the section, including the highest

719   abundance of warm-water taxa and % planktic foraminifera (Fig. 12 d, e), increasing nannofossil and

720   dinocyst diversity, and a long-term shift to more abundant and diverse angiosperm vegetation (Fig. 7).

721   Declining SST from late EECO to post-EECO is mirrored with an increasing abundance of cool-water

722   nannofossil and dinocyst taxa, although terrestrial vegetation shows little change in the post-EECO

723   Heretaungan. It is not until the Bortonian that cooler temperatures are indicated by the rise in

724   abundance of the Nothofagaceae, southern beech, family.

725

726   *6.2 Early and middle Eocene sedimentation changes*

727   Early Eocene extreme warming events are commonly linked with increased accumulation of

728   terrigenous material on continental margins, including New Zealand, due to an enhanced hydrological

729   cycle that promoted both chemical and physical weathering processes and transport of terrigenous

730   sediment into adjacent basins (Dickens et al., 1997; Schmitz and Pujalte, 2007; Carmichael et al.,

2017). This is well-documented for the short-lived PETM, which is also associated with notable

changes in sedimentation patterns and marine primary productivity (Crouch et al., 2003; Nicolo et al.,

2007; Giusberti et al., 2016). Equivalent EECO records are sparse, making it difficult to compare the

climatic impacts on sedimentation between transient and long-term warming events. In New Zealand,

the Mead and Branch Stream (Fig. 1) records suggests similar changes in terrigenous delivery and

sedimentation occurred in the EECO to that documented for the PETM, with an increased component

of terrigenous-sourced clay during early Eocene CIEs, as well as in the EECO, and highest sediment

accumulation rates (SARs) during the EECO (Slotnick et al., 2012, 2015; Dallanave et al., 2014).

At mid-Waipara, SARs also appear to have increased at the base of the EECO (from ~4 to 10

m/Myr), peaked in the latest EECO (14 m/Myr), and then stabilised through the overlying post-EECO

Heretaungan (~10 m/Myr; Dallanave et al., 2016). However, SAR estimates are uncertain for the base

of the section due to limited exposure, and in the late Heretaungan due to likely erosion at the

overlying unconformity (~59 m). The SAR is generally much higher at Mead Stream (Dallanave et

al., 2014), despite the sediments being primarily pelagic carbonate and hemipelagic clays; background

SAR is 20 m/Myr and peak SAR in the EECO is 40–100 m/Myr at Mead Stream. This indicates that

the Eocene section at mid-Waipara is relatively condensed and that cryptic unconformities may be

present, which would distort the estimates of SAR.

Two other commonly used proxies for terrigenous input in marine sediments, the BIT index

and terrestrial palynomorph abundance (Fig. 12f), exhibit opposing trends in the lower part of the

early Eocene. This may be related to other factors influencing the BIT index, as discussed above

(section 5.3). However, the convergence of trends in the mid–late EECO and post-EECO Heretaungan

suggests that cooling is linked to increased terrigenous input in this section.

In this respect, the mid-Waipara record differs from Mead Stream, where a notable increase in

accumulation of terrigenous material is associated with the long-term EECO. This is further

emphasised by differences in thickness of the EECO at the two sections: 34 m at mid-Waipara versus

>100 m at Mead Stream (Supp. Information Fig. 2). Benthic foraminiferal assemblages indicate both

sections were deposited at bathyal depths in the early Eocene. Studies of the eastern Marlborough

758   pelagic succession (Reay, 1993; Hollis et al., 2005b) show that Mead Stream is the thickest, and most

759   distal, Paleocene–Eocene section of an oceanic carbonate ramp succession. Sections closer to the

760   paleo-shoreline are thinner, with major unconformities truncating the succession in this proximal area.

761   A similar relation may apply to Mead and mid-Waipara sections, with Mead being in a distal

762   depocenter for terrigenous weathering products in the EECO, whereas mid-Waipara represents a more

763   dynamic coastal setting, where climatic changes cause changes in sediment delivery pathways and

764   result in a more complex relationship between SAR and other indicators of terrigenous supply, sea

765   level change and climate.

766

767   *6.3 Early and middle Eocene changes in marine productivity and surface water conditions*

768   Marine microfossils can provide insight into surface productivity and nutrient availability.

769   Peridinioid dinocysts, predominantly heterotrophic dinoflagellates, make up <20% of the assemblage

770   in the lower–mid EECO, and the abundance peak (40%) in the late EECO is coincident with an

771   increase in the BIT index and terrestrial palynomorph abundance (Fig. 12f, g). Peridinioid abundance

772   is <30% of the assemblage in the post-EECO. The lowest peridinioid abundance is associated with the

773   negative CIEs and high SST (correlation r = 0.39, p <0.02 and r = -0.3, p <0.01, n = 43, with $\delta^{13}C$ and

774   TEX_{86}, respectively).

775   Several short-lived abundance peaks, up to 30%, of the genus *Homotryblium* in the early and

776   middle EECO (Fig. 12e) suggest the presence of seasonally elevated salinity levels and/or surface

777   water stratification (Frieling and Sluijs, 2018). *Homotryblium* is morphologically like the extant

778   euryhaline species *Polysphaeridium zoharyi*, which occurs in low–mid latitudes and is tolerant to

779   extreme salinities and shallow water depths (Edwards and Anderle, 1992; Reichart et al., 2004). Most

780   studies suggest *Homotryblium* has an affinity to hypersaline environments (Köthe, 1990; Pross and

781   Schmiedl, 2002), although there is a possibility the genus favoured low-salinity conditions (Dybkjær,

782   2004). Whilst super-abundant *Homotryblium* is commonly linked with lagoonal/restricted inner

783   marine settings (e.g., de Verteuil and Norris, 1996), benthic foraminiferal assemblages show the

784   Ashley Mudstone was deposited at bathyal depths. The *Homotryblium* peaks do not correlate with

785 inner neritic dinocyst increases (e.g., *Cordosphaeridium*, *Glaphyrocysta*; Fig. 7), suggesting the

786 surface water conditions that led to *Homotryblium* blooms were not restricted to a coastal setting but

787 extended into the Canterbury Basin. The EECO *Homotryblium* peaks correspond with high SST and

788 %GDGT$_{RS}$ values >30 (Fig. 12 b, c), and partly correlate with CIEs (#3 and #4) and peaks in warm-

789 water nannofossils (Figs. 12a, d). Elsewhere, high %GDGT$_{RS}$ values (>30) are seen in times of

790 elevated warmth (PETM and EECO) from the North Sea Basin, New Jersey margin and SW Pacific

791 sites that have coeval high abundances of epicystal Goniodomidae dinocysts, such as *Eocladopyxis,*

792 *Polysphaeridium* and *Homotryblium* (Sluijs and Brinkhuis, 2009; Inglis et al., 2015; Frieling and

793 Sluijs, 2018). In New Zealand, abundant *Homotryblium* is also noted in the EECO at Mead Stream

794 (Cooper, 2018) and Hampden Beach (Inglis et al., 2015).

795   While deciphering the influence of productivity on nannofossil assemblages is complicated by

796 the interconnectivity between temperature and nutrient availability (Agnini et al., 2007; Schneider et

797 al., 2011), some general observations indicate that surface productivity at mid-Waipara did not

798 increase in the EECO. Rather, the EECO is characterised by the replacement of one mesotrophic

799 genus, *Toweius*, with another, *Reticulofenestra*, which occurs in the late EECO and is coeval with the

800 peridinioid abundance peak and increasing BIT values and terrestrial palynomorph abundance (Fig.

801 12f, g). The combined abundance of *Toweius* and *Reticulofenestra* is lower in the EECO (average

802 46%) than it is below or above the EECO (average 65% and 55%, respectively).

803   At the oceanic bathyal Mead Stream, there is evidence for increased terrigenous-sourced clay

804 content and SARs in the EECO (Slotnick et al., 2012; Dallanave et al., 2015), but no clear signal of

805 enhanced marine surface productivity. A marked decline in radiolarian abundance and diversity, and

806 low diatom abundance, imply a decrease in biosiliceous productivity linked with the EECO (Hollis,

807 2006). Rather, assemblages characteristic of oligotrophic, possibly stratified, conditions prevailed.

808 Open ocean gonyaulacoid taxa dominate dinocyst assemblages in the EECO, and super-abundant

809 *Homotryblium* occurs in an interval corresponding with the J-event (EECO onset; Cooper, 2018).

810

811 *6.4 Early Eocene vegetation change*

In New Zealand, the most notable long-term vegetation shift in the early Eocene is the widespread abundance increase in Casuarinaceae pollen of *Myricipites harrisii* (Raine, 1984; Pocknall, 1990; Crouch and Brinkhuis, 2005). The precise timing is poorly constrained due to difficulties in accurately dating terrestrial sediments and correlation with well-calibrated marine sections (Morgans et al., 2004; Raine et al., 2009; Handley et al., 2011). The vegetation shift has been correlated with middle–late Waipawan, nannofossil Zone NP11 and dinocyst zone NZE3 (Crouch and Brinkhuis, 2005), but a direct link with Eocene climatic changes has not been made until this study.

Our results provide the clearest evidence to date that the Casuarinaceae increase is correlated with EECO warming. The increase in *M. harrisii* abundance is in the late Waipawan (Fig. 8), and corresponds with the warmest SST in the early EECO (Fig. 12b). Casuarinaceae remain frequent–abundant in the EECO, and whilst there is a gradual decline in abundance post-EECO, the duration of common–abundant *M. harrisii* continues at least 4–5 Myr above the EECO and into the middle Eocene Porangan Stage (Raine et al., 2009).

Pollen of *M. harrisii* is first seen in New Zealand and Australia in the early–middle Paleocene (Raine, 1984; Macphail et al., 1994; Contreras et al., 2014), but is relatively sparse until the early Eocene. Whilst *M. harrisii* is common or abundant in New Zealand in the early–middle Eocene, the southern Australia record is varied: high abundances occur in the Australo-Antarctic basins (e.g., Otway Basin) but not in Southeastern Australia (e.g., Gippsland Basin), where gymnosperm pollen remain abundant (Harris, 1965; Carpenter et al., 2012; Contreras et al., 2014; Holdgate et al., 2017). Casuarinaceae is a family characteristic of sclerophyllous, seasonally dry forests, but also includes the primitive genus *Gymnostoma*, a tropical–subtropical rainforest margin taxon adapted to low nutrient soils (Hill, 1994; Prider and Christophel, 2000; Steane et al., 2003). Fossil pollen of *Gymnostoma* and *Casuarina* are virtually indistinguishable, apart from the latter being generally larger (Kershaw, 1970). Whilst macrofossil evidence suggests *Gymnostoma* was common in the early Paleogene (Christophel, 1980; Hill, 1994; Greenwood and Christophel, 2005), the earliest macrofossil record of *Casuarina* is less clear, perhaps in the Eocene, but the oldest definitive macrofossils are Oligocene (Greenwood and Christophel, 2005; McGowran and Hill, 2015). The ecological interpretation of *M.*

839 *harrisii* is therefore complicated by the possibility that pollen was produced by *Gymnostoma* and

840 *Casuarina* plants.

841   A combination of causes may have led to the long-term increase in Casuarinaceae vegetation

842 linked with the EECO in New Zealand. Firstly, transient extreme warming at the PETM did not have

843 a notable effect on Casuarinaceae (Crouch and Brinkhuis, 2005), but longer-term warming associated

844 with the EECO may have allowed for vegetation change to occur and become established. At mid-

845 Waipara, EECO mean annual temperature (MAT) estimates have been calculated from spore and

846 pollen assemblages, which range from $17.1 \pm 6.8°C$ (bioclimatic analysis) to $22.6 \pm 1.4°C$ (co-

847 existence approach) in the EECO (Pancost et al., 2013). MAT estimates are lower than geochemical-

848 based SST proxies (Fig. 10; Hollis et al., 2019). Secondly, precipitation changes may have led to

849 conditions well-suited to Casuarinaceae. Hydrogen isotopes of plant biomarkers ($\delta D_{n\text{-alkane}}$) from the

850 Kumara-2 core (Fig. 1) show a general increase in the early Eocene, with highest values (-135‰)

851 coeval with the *M. harrisii* increase, perhaps suggesting a more seasonal climate or increasing aridity

852 (Handley et al., 2011). Moreover, long-term changes in temperature and precipitation patterns may

853 have led to changes in soil conditions more favourable for Casuarinaceae. Results from the Taranaki

854 Basin (Fig. 1) indicate enhanced chemical weathering in the early Eocene (Zone MH1), with

855 increased quartz-K-feldspar sediments and a decline in plagioclase-rich sediments (Higgs et al.,

856 submitted).

857

858 **7. Conclusions**

859   The early Paleogene succession at mid-Waipara River, Canterbury Basin, New Zealand, has

860 been the focus of several high-profile paleoclimate studies as the sediments contain good preservation

861 of microfossils and organic biomarkers. Here, we build on this previous work and undertake a

862 quantitative analysis of paleontological and multiproxy geochemical indicators of climate and

863 environmental change through the early–middle Eocene, with particular focus on the Early Eocene

864 Climatic Optimum (EECO).

865   The section spans the early Eocene (New Zealand Waipawan Stage) to middle Eocene (lower

866   Bortonian Stage), ~55.5–42.5 Ma, with a non-exposed interval in the lower Eocene (middle

867   Waipawan) and an unconformity, spanning ~3 Myr, in the middle Eocene (latest Heretaungan,

868   Porangan and earliest Bortonian Stages). The EECO corresponds with a ~33.5 m interval from late

869   Waipawan to the Mangaorapan/Heretaungan boundary, 49.27 Ma, in upper Chron C22n. The EECO

870   onset is not captured as it occurs in the non-exposed interval, but the termination is preserved and

871   corresponds to a sustained shift to lower TEX_{86} values and more positive bulk carbonate $\delta^{13}C$ values.

872   A series of six negative CIEs are identified in the EECO and tentatively correlated with named CIEs

873   in global benthic $\delta^{13}C$ compilations. These CIEs are found to be associated with high TEX_{86} values,

874   indicating that they represent hyperthermals.

875   The TEX_{86} record indicates that SST increased from the earliest Eocene to the early EECO,

876   by 7°C with the TEX_{86}^{H} calibration and by 12°C with the BAYSPAR calibration. Peak SST for the

877   EECO were 34°C (TEX_{86}^{H} calibration) and 36°C (BAYSPAR calibration). SST began to gradually

878   decline from the middle EECO (~51 Ma) and reached minimum values for the post-EECO

879   Heretaungan at ~47 Ma (27°C and 22°C, respectively). Similar average values are recorded for the

880   overlying Bortonian Stage, but with significant variation in SST estimates of 6–8°C. This SST record

881   is in good agreement with previous estimates from a lower resolution sample set using TEX_{86} and

882   planktic foraminiferal $\delta^{18}O$ and Mg/Ca ratios (Hollis et al., 2009, 2012; Creech et al., 2010).

883   We also find good agreement between the relative temperature trend for TEX_{86} and trends in

884   marine microfossil proxies for temperature, providing confidence that both approaches are useful

885   guides to past water temperature. Pronounced warming in the early EECO corresponds with the most

886   pronounced biotic changes in the section. This includes increased diversity in calcareous nannofossil

887   and dinocyst assemblages, the highest abundance of warm-water taxa and planktic foraminifera, and a

888   long-term shift to abundant and diverse angiosperm vegetation, primarily driven by a rise in

889   Casuarinaceae. Marine microfossils also offer a means to evaluate the inference drawn from

890   geochemical proxies that latitudinal temperature gradients were greatly reduced in the EECO. Our

891   provisional analysis of microfossil assemblages indicates the latitudinal temperature gradient between

mid- and low latitudes in the EECO was greater than that indicated by geochemical SST proxies. Further biogeographic studies of microfossil assemblages are needed to determine if it is possible to quantify these gradients.

There is no clear evidence for a notable increase in sedimentation rates or accumulation of terrigenous material associated with warmest temperatures of the EECO. This contrasts with that previously documented at the nearby oceanic carbonate Mead Stream section and may reflect different sediment delivery pathways and a more dynamic coastal mid-Waipara setting. Marine surface productivity does also not appear to have increased in the warmest part of the EECO, although superabundant *Homotryblium*, a euryhaline dinocyst genus, in the early and middle EECO suggest the presence of seasonally elevated salinity levels and/or stratified surface waters. In the late EECO, from ~50 Ma, combined proxies indicate declining temperatures correspond with an increase in cool-water marine taxa and contribution of terrigenous material into the Canterbury Basin, which continued into the post-EECO.

This multi-proxy study of the continental margin mid-Waipara River section shows the value of combining well-calibrated biological and geochemical records to better constrain and understand past warm climate states, and to provide a robust means to interrogate geochemical-based temperature proxies (Hollis et al., 2019).

Figures

918 **Figures**

919 **1.** Location of the mid-Waipara River section in northeast South Island (A), and early Eocene (50 Ma)

920 paleogeographic reconstruction for the Southwest Pacific based on the paleomagnetic reference frame

921 of Matthews et al. (2016) (B). Thick red line in (A) shows the position of Ashley Mudstone samples

922 examined in this study. HB = Hampden Beach, KC = Kumara-2 core, TB = Taranaki Basin.

923

924 **2.** The early and middle Eocene timescale (GTS2014, after Gradstein et al. 2012; Ogg et al., 2014;

925 NZGTS2015, after Raine et al., 2015) and global benthic foraminiferal isotope record (Cramer et al.,

926 2009; recalibrated to GTS2014). The age of the Mangaorapan/Heretaungan boundary is recalibrated

927 to Westerhold et al. (2017). Ages of calcareous nannofossil (NP) zone boundaries are based on

928 Gradstein et al. (2012), with adjustments to Zones NP9 to NP14 after Hollis et al. (2019). The New

929 Zealand dinocyst and spore/pollen zones are from Wilson et al. (1988) and Morgans et al. (2004); *C.*

930 *col = Charlesdowniea coleothrypta*, *C. ed = Charlesdowniea edwardsii*, *M. pe = Membranophoridium*

931 *perforatum*, *W. ec = Wilsonidium echinosuturatum*). Grey bands represent the position of the

932 Paleocene–Eocene Thermal Maximum (PETM) and Early Eocene Climatic Optimum (EECO).

933

934 **3.** Summary of the mid-Waipara River lithological column (Ashley Mudstone), and ranges of

935 biostratigraphic marker taxa and biozones in the early to middle Eocene. Also shown are the

936 stratigraphic distribution of samples taken from the Ashley Mudstone for both the 2007 and 2012

937 collections, and planktic foraminiferal abundance (%). Thickened lines indicate intervals of common

938 (>8%) abundance. Magnetostratigraphy from Dallanave et al. (2016), NP zones are calcareous

939 nannofossil zones.

940

941 **4.** Variation in calcium carbonate (CaCO₃) content (a), and calcareous nannofossil preservation (b),

942 diversity (c) and relative abundance of biogeographic indicator taxa (d) in the mid-Waipara River

943 section. Preservation indicators include visually observed preservation (VOP, black line and markers)

944 and relative abundance of *Zygrhablithus bijugatus* (red line and markers), a species sensitive to

945 dissolution. Diversity is indicated by taxon richness (black line and markers) and the Shannon

946 diversity index (red line and markers). Relative abundance of cool- and warm-water calcareous

947 nannofossil groups is shown, including selected cool (*Chiasmolithus* spp. and *Reticulofenestra*

948 *daviesii*) and warm-water (*Discoaster* spp., *Spenolithus* spp., and *Coccolithus formosus*) taxa. Shaded

949 intervals show the position of the Early Eocene Climatic Optimum (EECO, light grey) and the

950 negative carbon isotope excursions (numbered 1 to 6, dark grey).

951

952 **5.** Variation in calcium carbonate ($CaCO_3$) content (a), bulk carbonate $\delta^{13}C$ (b), TEX_{86} (c), and BIT

953 Index (d) for the early and middle Eocene in the mid-Waipara River section. Shaded intervals show

954 the position of the Early Eocene Climatic Optimum (EECO, light grey) and the negative carbon

955 isotope excursions (numbered 1 to 6, dark grey).

956

957 **6.** The mid-Waipara River bulk carbonate $\delta^{13}C$ and TEX_{86} records (b) compared with the benthic

958 foraminiferal stable isotope compilation (a) for North Pacific ODP Site 1209 and South Atlantic ODP

959 sites 1258, 1262 and 1263 of Westerhold et al. (2018), calibrated to the timescale of Westerhold et al.

960 (2017). Grey band and dashed lines represent the Early Eocene Climatic Optimum (EECO) and

961 carbon isotope excursions (CIEs). The six CIEs at mid-Waipara River are tentatively correlated with

962 named CIEs as indicated.

963

964 **7.** The relative abundance of selected dinocyst species and genera from the early and middle Eocene

965 in the mid-Waipara River section. Gonyaulacoid dinocysts are shown in dark grey; peridinioid

966 dinocysts in light grey. The relative abundances of total peridinioid dinocysts and climate indicator

967 taxa are also shown. Shaded bands represent the Early Eocene Climatic Optimum (EECO, light grey)

968 and the negative carbon isotope excursions (dark grey).

969

970 **8.** The relative abundance of total terrestrial palynomorphs, selected spore and pollen species and

971 genera, and relative proportions of spore, gymnosperm and angiosperm groups from the early and

972 middle Eocene in the mid-Waipara River section. Shaded bands represent the Early Eocene Climatic

973 Optimum (EECO, light grey) and the negative carbon isotope excursions (dark grey).

974

975 **9.** Temperature variation and associated parameters in the early and middle Eocene at mid-Waipara

976 River section: sea surface temperature (SST) record using BAYSPAR and TEX_{86}^{H} calibrations, with

977 95% confidence band for BAYSPAR (a), relative temperature change of SST (BAYSPAR and

978 TEX_{86}^{H}) (b), and %$GDGT_{RS}$ (c). Shaded bands represent the Early Eocene Climatic Optimum (EECO,

979 light grey) and the negative carbon isotope excursions (dark grey).

980

981 **10.** Summary of available isoGDGT- and foraminifera-based SST estimates from the early and middle

982 Eocene at mid-Waipara River, calibrated to the timescale of Westerhold et al. (2017). SSTs are

983 derived from TEX_{86} using BAYSPAR (this study) and TEX_{86}^{H} calibrations (this study and Hollis et

984 al., 2012). Foraminifera-based SST estimates are from Mg/Ca ratios and $\delta^{18}O$ values of the mixed

985 layer planktic genus *Morozovella* (Hollis et al., 2012, 2019). SST derived from the TEX_{86}^{H} and

986 BAYSPAR calibrations are warmer in some intervals than SST calculated from mixed layer

987 foraminifera (Mg/Ca ratios and $\delta^{18}O$ values), and this wider variation in $\delta^{18}O$-based SST is thought to

988 reflect diagenetic effects (Hollis et al., 2012). Error bars are ± 2.5°C TEX_{86}^{H} and 1 sigma for Mg/Ca

989 and $\delta^{18}O$; 95% confidence interval for BAYSPAR is shaded light blue. Shaded bands represent the

990 Early Eocene Climatic Optimum (EECO, light grey) and negative carbon isotope excursions (dark

991 grey).

992 **11.** The relative abundance of key calcareous nannofossil warm-water and cool-water taxa and genera

993 from selected subtropical (Site 1210, Shatsky Rise, Northwest Pacific Ocean), temperate (Site 762,

994 Exmouth Plateau, Indian Ocean; mid-Waipara River, Canterbury Basin; Site 277, Campbell Plateau),

995 and polar (Site 1135, Kerguelen Plateau, Southern Indian Ocean) provinces. Data for sites 762, 1135

996   and 1210 are from Schneider et al. (2011). Data are recalibrated to Gradstein et al. (2012). Sites are

997   shown on a paleogeographic reconstruction for the early Eocene, using the same reference frame as in

998   Fig. 1 (Matthews et al., 2016). The shaded band represents the Early Eocene Climatic Optimum

999   (EECO).

1000   **12.** Summary of climate and environmental proxies for the mid-Waipara River section, plotted against

1001   age (Westerhold et al., 2017). Bulk carbonate $\delta^{13}C$ record (a), TEX_{86}-derived SST based on

1002   BAYSPAR and TEX_{86}^{H} calibrations (b), % Red Sea GDGTs (c), calcareous nannofossil warm- and

1003   cool-water groups and % planktic foraminifera (d), dinocyst warm- and cooler-water groups (e), BIT

1004   index and % terrestrial palynomorphs (f), and calcareous nannofossil taxa and dinocyst peridinioids

1005   thought to be surface productivity indicators (g). Shaded bands represent the Early Eocene Climatic

1006   Optimum (EECO, light grey) and negative carbon isotope excursions (dark grey).

References

Agnini, C., Fornaciari, E., Rio, D., Tateo, F., Backman, J., Giusberti, L., 2007. Responses of calcareous nannofossil assemblages, mineralogy and geochemistry to the environmental perturbations across the Paleocene/Eocene boundary in the Venetian Pre-Alps. Marine Micropaleontology 63, 19–38, doi: 10.1016/j.marmicro.2006.10.002.

Agnini, C., Fornaciari, E., Raffi, I., Catanzariti, R., Pälike, H., Backman, J., et al., 2014. Biozonation and biochronology of Paleogene calcareous nannofossils from low and middle latitudes. Newsletters on Stratigraphy 47, 131–181.

Anagnostou, E., John, E.H., Edgar, K.M., Foster, G., Ridgwell, A., Inglis, G.N., Pancost, R.D., Lunt, D.J., Pearson, P.N., 2016. Changing atmospheric CO_2 concentration was the primary driver of early Cenozoic climate. Nature, doi:10.1038/nautre17423.

Aubry, M.-P., 1991. Sequence stratigraphy: Eustasy or tectonic imprint? Journal of Geophysical Research 96, 6641–6679, doi: 10.1029/90JB01204.

Awad, W.K., Oboh-Ikuenobe, F.E., 2016. Early Paleogene dinoflagellate cysts from ODP Hole 959D, Côte d'Ivoire-Ghana Transform Margin, West Africa: new species, biostratigraphy and paleoenvironmental implications. Journal of African Earth Sciences 123, 123–144.

Backman, J., 1986. Late Paleocene to middle Eocene calcareous nannofossil biochronology from the Shatsky Rise, Walvis Ridge and Italy. Palaeogeography, Palaeoclimatology, Palaeoecology 57, 43–59.

Barnet, J.S.K., Littler, K., Westerhold, T., Kroon, D., Leng, M.J., Bailey, I., Röhl, U., Zachos, J.C., 2019. A high-fidelity benthic stable isotope record of Late Cretaceous–Early Eocene climate change and carbon-cycling. Paleoceanography and Paleoclimatology 34, 672–679. https://doi.org/10.1029/2019PA003556.

Beerling, D.J., Royer, D.L., 2011. Convergent Cenozoic CO_2 history. Nature Geosciences 4, 418–420.

Bijl, P.K., Schouten, S., Sluijs, A., Reichart, G.-J., Zachos, J.C., Brinkhuis, H., 2009. Early Paleogene temperature evolution of the southwest Pacific Ocean. Nature 461, 776–779.

Bijl, P.K., Pross. J., Warnaar, J., Stickley, C., Huber, M., Guerstein, R., Houben, A.J.P., Sluijs, A., Visscher, H., Brinkhuis, H., 2011. Environmental forcings of Paleogene Southern Ocean dinoflagellate biostratigraphy. Paleoceanography 26, PA1202, doi:10.1029/2009PA001905.

Bijl, P.K., Sluijs, A., Brinkhuis, H., 2013a. A magneto- and chemostratigraphically calibrated dinoflagellate cyst zonation of the early Paleogene South Pacific Ocean. Earth-Science Reviews 124, 1–31.

Bijl, P.K., Bendle, J., Boharty, S., Pross. J., Schouten, S., Tauxe, L., Stickley, C., McKay, R., Röhl, U., Olney, M., Sluijs, A., Escutia, C., Brinkhuis, H., and Expedition 318 Scientists, 2013b. Eocene cooling linked to early flow across the Tasmanian Gateway. Proceedings of the national Academy of Science U.S.A 110, 9645–9650.

Bown, P. R., 1998. Calcareous Nannofossil Biostratigraphy. Cambridge University. 315 p.

Bown, P. R., 2005. Paleogene calcareous nannofossils from the Kilwa and Lind areas of coastal Tanzania (Tanzania Drilling Project 2003–4). Journal of Nannoplankton Research 27, 21–95.

Bown, P. R., Young, J. R., 1998. Techniques. *In* Bown, P. R. (Ed.), Calcareous Nannofossil Biostratigraphy. London: Kluwer Academic Publishers, 16–28.

Boudreau, B., Middelburg, J., Sluijs, A., van der Ploeg, R., 2019. Secular variations in the carbonate chemistry of the oceans over the Cenozoic. Earth Planetary Science Letters 512, 194–206.

Bralower, T. J., 2002. Evidence of surface water oligotrophy during the Paleocene–Eocene thermal maximum: Nannofossil assemblage data from Ocean Drilling Program Site 690, Maud Rise, Weddell Sea. Paleoceanography 17, doi: 10.1029/2001pa000662.

Brinkhuis, H., 1994. Late Eocene to Early Oligocene dinoflagellate cysts from the Priabonian type-area (northeast Italy): biostratigraphy and paleoenvironmental interpretation. Palaeogeography, Palaeoclimatology, Palaeoecology 107, 121–163.

Carlson, H., Caballero, R., 2017. Atmospheric circulation and hydroclimate impacts of alternative warming scenarios for the Eocene. Climates of the Past 13, 1037–1048.

Carmichael, M., Inglis, G., Badger, M., Naafs, B.D., Behrooz, L., Remmelzwaal, S., Monteiro, F., Rohrssen, M., Farnsworth, A., Buss, H., Dickson, A., Valdes, P., Lunt, D., Pancost, R.D., 2017. Hydrological and associated biogeochemical consequences of rapid global warming during the Paleocene–Eocene Thermal Maximum. Global and Planetary Change 157, 114–138.

Carpenter, R.J., Jordan, G.J., Macphail, M.K., Hill, R.S., 2012: Near-tropical Early Eocene terrestrial temperatures at the Australo-Antarctic margin, western Tasmania. Geology 40, 267–270.

Christophel, D.C., 1980: Occurrence of *Casuarina* megafossils in the Tertiary of South-eastern Australia. Australian Journal of Botany 27, 249–259.

Contreras, L., Pross, J., Bijl, P.K., O'Hara, R.B., Raine, J.I., Sluijs, A., Brinkhuis, H., 2014: Southern high-latitude terrestrial climate change during the Paleocene–Eocene derived from a marine pollen record (ODP Site 1172, East Tasman Plateau). Climate of the Past 10, 1401–1420.

Cooper, R.A. (editor), 2004. The New Zealand Geological Timescale. Institute of Geological and Nuclear Sciences Monograph 22. 284p.

Cooper, T.F., 2018. Early Eocene palynology from Mead Stream, New Zealand. Master of Science (Geology) thesis, Victoria University of Wellington, December 2017.

Cramer, B., Wright, J.D., Kent, D.V., Aubry, M.-P., 2003. Orbital climate forcing of $\delta^{13}C$ excursions in the late Paleocene–early Eocene. Paleoceanography 18, 1097, doi:10.1029/2003PA000909.

Cramer, B., Toggweiler, J.R., Wright, J.D., Katz, M.E., Miller, K.G., 2009. Ocean overturning since the Late Cretaceous: Inferences from a new benthic foraminiferal isotope compilation. Paleoceanography 24, PA4216, doi:10.1029/2008PA001683.

Cramwinckel, M.J., Huber, M., Kocken, I., Agnini, C., Bijl, P., Bohaty, S., Frieling, J., Goldner, A., Hilgen, F., Kip, E., Peterse, F., van der Ploeg, R., Röhl, U., Schouten, S., Sluijs, A., 2018. Synchronous tropical and polar temperature evolution in the Eocene. Nature, doi.org/10.1038.s41586-018-0272-2.

Creech, J.B., Baker, J., Hollis, C.J., Morgans, H.E.G., Smith, E., 2010. Eocene sea temperatures for the mid-latitude southwest Pacific from Mg/Ca ratios in planktonic and benthic foraminfera. Earth and Planetary Science Letters 299, 483–495.

Crouch, E.M., Brinkhuis, H., 2005: Environmental change across the Paleocene–Eocene transition from eastern New Zealand: a marine palynological approach. Marine Micropaleontology 56, 138–160.

Crouch, E.M., Heilmann-Clausen, C., Brinkhuis, H., Morgans, H., Rogers, K., Egger, H., Schmitz, B., 2001. Global dinoflagellate events associated with the late Paleocene thermal maximum. Geology 29, 315–318.

Crouch, E.M., Brinkhuis, H., Visscher, H., Adatte, T., Bolle, M.-P., 2003. Late Paleocene–early Eocene dinoflagellate cyst records from the Tethys: further observations on the global distribution of *Apectodinium*. Geological Society of America Special Paper 369, 113–131.

Crouch, E.M., Dickens, G.R., Brinkhuis, H., Aubry, M.-P., Hollis, C.J., Rogers, K.M., Visscher, H., 2003. The *Apectodinium* acme and terrestrial discharge during the Paleocene–Eocene thermal maximum: new palynological, geochemical and calcareous nannoplankton observations at Tawanui, New Zealand. Palaeogeography, Palaeoclimatology, Palaeoecology 194, 387–403.

Dale, B., 1996. Dinoflagellate cyst ecology: modelling and geological applications. In: Jansonius, J, McGregor, D.C. (Eds.), Palynology: Principles and Applications. AASP Foundation, 1249–1275.

Dallanave, E., Agnini, C., Bachtadse, V., Muttoni, G., Crampton, J.S., Strong, C.P., Hines, B.R., Hollis, C.J., Slotnick, B.S., 2015. Early to middle Eocene magneto-biochronology of the southwest Pacific Ocean and climate influence on sedimentation: Insights from the Mead Stream section, New Zealand. Geological Society of America Bulletin 127, 643–660.

Dallanave, E., Bachtadse, V., Crouch, E.M., Tauxe, L., Shepherd, C.L., Morgans, H.E.G., Hollis, C.J., Hines, B.R., Sugisaki, S., 2016. Constraining early to middle Eocene climate evolution of the southwest Pacific and Southern ocean. Earth and Planetary Science Letters 433, 380–392.

De Jonge, C., Hopmans, E.C., Stadnitskaia, A., Rijpstra, W.I.C., Hofland, R., Tegelaar, E., Sinninghe Damsté, J.S., 2013: Identification of novel penta- and hexamethylated branched glycerol dialkyl glycerol tetraethers in peat using HPLC–MS^2, GC–MS and GC–SMB-MS. Organic Geochemistry 54, 78-82, doi: 10.1016/j.orggeochem.2012.10.004.

De Jonge, C., Hopmans, E.C., Zell, C.I., Kim, J.-H., Schouten, S., Sinninghe Damsté, J.S., 2014a: Occurrence and abundance of 6-methyl branched glycerol dialkyl glycerol tetraethers in soils: implications for palaeoclimate reconstruction. Geochimica et Cosmochimica Acta 141, 97-112, doi: 10.1016/j.gca.2014.06.013.

De Jonge, C., Stadnitskaia, A., Hopmans, E.C., Cherkashov, G., Fedotov, A., Sinninghe Damsté, J.S., 2014b. In situ produced branched glycerol dialkyl glycerol tetraethers in suspended particulate matter from the Yenisei River, Eastern Siberia. Geochimica et Cosmochimica Acta 125, 476-491.

De Vernal, A., Eynaud, F., Henry, M., Hillaire-Marcel, C., Londeix, L., Mangin, S., Matthiessen, J., Marret, F., Radi, T., Rochon, A., Solignac, S., Turon, J., 2005. Reconstruction of sea-surface conditions at middle to high latitudes of the Northern Hemisphere during the Last Glacial maximum (LGM) based on dinoflagellate cyst assemblages. Quaternary Science Reviews 24, 897–924.

De Verteuil, L., Norris, G., 1996. Middle to upper Miocene *Geonettia clinae*, an opportunistic coastal embayment dinoflagellate of the *Homotryblium* complex. Micropaleontology 42, 263–284.

Dickens, G.R., Castillo, M., Walker, J., 1997. A blast of gas in the latest Paleocene: simulating first-order effects of massive dissociation of oceanic methane hydrate. Geology 25, 259–262.

Dunkley Jones, T., Bown, P. R., Pearson, P. N., 2009. Exceptionally well preserved upper Eocene to lower Oligocene calcareous nannofossils (Prymnesiophyceae) from the Oande Formation (Kilwa Group), Tanzania. Journal of Systematic Paleontology 7, 359–411.

Dybkjær, K., 2004. Morphological and abundance variations in *Homotryblium*-cyst assemblages related to depositional environments; uppermost Oligocene–Lower Miocene, Jylland, Denmark. Palaeogeography, Palaeoclimatology, Palaeoecology 206, 41–58.

Edwards, L.E., Andrele, V., 1992. Distribution of selected dinoflagellate cysts in modern marine sediments. *In*: Head, M., Wrenn, J. (eds.), Neogene and Quaternary Dinoflagellate Cysts and Acritarchs. American Association of Stratigraphic Palynologists, Texas, p. 250–273.

Evans, D., Sagoo, N., Renema, W., Cotton, L., Müller, W., Todd, J., Saraswati, P.K., Stassen, P., Ziegler, M., Pearson, P., Valdes, P., Affek, H., 2018. Eocene greenhouse climate revealed by coupled clumped isotope-Mg/Ca thermometry. Proceedings of the National Academy of Sciences, 10.1073/pnas.1714744115.

Frieling, J., Iakovleva, A., Reichart, G.-J., Aleksandrova, G., Gnibidenko, Z., Schouten, S., Sluijs, A., 2014. Paleocene–Eocene warming and biotic response in the epicontinental West Siberian Sea. Geology 42, 767–770.

Frieling, J., Sluijs, A., 2018. Towards quantitative environmental reconstructions from ancient non-analogue microfossil assemblages: Ecological preferences of Paleocene–Eocene dinoflagellates. Earth-Science Reviews 185, 956–973.

Giusberti, L., Boscolo Galazzo, F., Thomas, E., 2016. Variability in climate and productivity during the Paleocene–Eocene Thermal Maximum in the western Tethys (Forada section). Climate of the Past 12, 213–240.

Gradstein, F. M., Ogg, J. G., Schmitz, M., Ogg, G., 2012. The Geologic Time Scale 2012. Elsevier, 1176 p.

Greenwood, D.R., Christophel, D 2005: The origins and Tertiary history of Austrlian "tropical" rainforests. *In*: Bermingham, E., Dick, C., Moritz, C. (eds.), Tropical Rainforests: past, present and future. University of Chicago Press, p. 336–373.

Guasti, E., Kouwenhoven, T.J., Brinkhuis, H., Speijer, R.P., 2005. Paleocene sea-level and productivity changes at the southern Tethyan margin (El Kef, Tunisia). Marine Micropaleontology 55, 1–17.

Handley, L, Crouch, E.M., Pancost, R.D., 2011: A New Zealand record of sea level rise and environmental change during the Paleocene–Eocene Thermal Maximum. Palaeogeography, Palaeoclimatology, Palaeoecology 305, 185–200.

Haq, B. U., 1981. Paleogene paleoceanography: early Cenozoic oceans revisited: Oceanologica Acta 4, supplement, 71-82.

Haq, B. U., Premoli-Silva, I., Lohmann, G.P., 1977. Calcareous plankton paleobiosgeographc evidence for major climatic fluctuations in the early Cenozoic Atlantic Ocean. Journal of Geohpysical Research 82, 3861–3876.

Harris, W.K., 1965: Basal Tertiary microflora from the Princetown area, Victoria, Australia. Palaeontographica Abt. B 115, 75–106.

Hayward, B.W., 1986. A guide to paleoenvironmental assessment using New Zealand Cenozoic foraminiferal faunas. New Zealand Geological Survey Report PAL 109. 73 p.

Hayward, B.W., Grenfell, H., Sabaa, A.T., Neil, H., Buzas, M., 2010. Recent New Zealand deep-water benthic foraminfiera: taxonomy, ecologic distribution, biogeography, and use in paleoenvironmental assessment. GNS Science Monograph 26. 363 p.

Hennissen, J., Head, M., Schepper, S., Groenveld, J., 2017. Dinoflagellate cyst paleoecology during Pliocene–Pleistocene climatic transition in the North Atlantic. Palaeogeography, Palaeoclimatology, Palaeoecology 470, 81–108.

Hernández-Sánchez, M.T., Woodward, E.M.S., Taylor, K.W.R., Henderson, G.M., Pancost, R.D., 2014: Variations in GDGT distributions through the water column in the South East Atlantic Ocean. Geochimica et Cosmochimica Acta 132, 337-348, doi: 10.1016/j.gca.2014.02.009.

Higgs, K.E., Munday, S., Forbes, A., Crouch, E., Sagar, M., submitted. A geochemical and biostratigraphic approach to investigating regional changes in sandstone composition through the Paleocene–Eocene, Taranaki Basin, New Zealand. Geological Magazine.

Hill, R.S., 1994: The history of selected Australian taxa. *In*: Hill, R.S. (ed.), History of the Australian vegetation: Cretaceous to Recent. Cambridge University Press, p. 390–419.

Hines, B.R., Hollis, C.J., Atkins, C.B., Baker, J.A., Morgans, H.E.G., Strong, C.P., 2017. Reduction of oceanic temperature gradients in the early Eocene Southwest Pacific Ocean. Palaeogeography, Palaeoclimatology, Palaeoecology 475, 41–54.

1176 Holdgate, G.R., Sluiter, I.R.K., Taglieri, J., 2017: Eocene–Oligocene coals of the Gippsland and Australo-
1177   Antarctic basins - paleoclimatic and paleogeographic context and implications for earliest Cenozoic
1178   glaciations. Palaeogeography, Palaeoclimatology, Palaeoecology 472, 236–255.
1179 Hollis, C.J., 2006. Radiolarian turnover through the Paleocene–Eocene transition, Mead Stream, New Zealand.
1180   Eclogae geol. Helv. 99 Supplement 1, S79–S99.
1181 Hollis, C.J., Dickens, G.R., Field, B., Jones, C.M., Strong, C.P., 2005a. The Paleocene–Eocene transition at
1182   Mead Stream, New Zealand: a southern Pacific record of early Cenozoic global change. Palaeogeography,
1183   Palaeoclimatology, Palaeoecology 215, 313–343.
1184 Hollis, C.J., Field, B., Jones, C.M., Wilson, G.J., Dickens, G.R., 2005b. Biostratigraphy and carbon isotope
1185   stratigraphy of uppermost Cretaceous–lower Cenozoic Muzzle Group in middle Clarence valley, New
1186   Zealand. Journal of the Royal Society of New Zealand 35, 345–383.
1187 Hollis, C.J., Handley, L., Crouch, E.M., Morgans, H.E.G., Baker, J.A., Creech, J.B., Collins, K.S., Gibbs, S.,
1188   Huber, M., Schouten, S., Pancost, R.D., Zachos, J.C., 2009. Tropical sea temperatures in the high-latitude
1189   South Pacific during the Eocene. Geology 37, 99–102.
1190 Hollis, C.J., Taylor, K.W.R., Handley, L., Pancost, R.D., Huber, M., Creech, J.B., Hines, B.R., Crouch, E.M.,
1191   Morgans, H.E.G., Crampton, J.S., Gibbs, S., Pearson, P.N., Zachos, J.C., 2012. Early Paleogene temperature
1192   history of the Southwest Pacific Ocean: Reconciling proxies and models. Earth and Planetary Science
1193   Letters 349-350, 53–66.
1194 Hollis, C.J., Tayler, M.S., Andrew, B,, Taylor, K.W., Lurcock, P., Bijl, P.B., Kulhanek, D.K., Crouch, E.M.,
1195   Nelson, C.S., Pancost, R.D., Huber, M., Wilson, G.S., Ventura, G.T., Crampton, J.S., Schiøler, P., Phillips,
1196   A., 2014. Organic-rich sedimentation in the South Pacific Ocean associated with Late Paleocene slimatic
1197   cooling. Earth-Science Reviews 134, 81–97.
1198 Hollis, C.J., Hines, B.R., Littler, K., Villasante-Marcos, V., Kulhanek, D.K., Strong, C.P., Zachos, J.C., Eggins,
1199   S.M., Northcote, L., Phillips, A., 2015. The Paleocene–Eocene Thermal maximum at DSDP Site 277,
1200   Campbell Plateau, southern Pacific Ocean. Climate of the Past 11, 1009–1025.
1201 Hollis, C.J., Dunkley Jones, T., Anagnostou, E., Bijl, P., Cramwinckel, M., Edgar, K, et al. 2019. The DeepMIP
1202   contribution to PMIP4: methodologies for selection, compilations and analysis of latest Paleocene and early
1203   Eocene climate proxy data. Geoscientific Model Devlopment, https://doi.org/10.5194/gmd-2018-309.
1204 Hopmans, E.C., Schouten, S., Sinninghe Damsté, J.S., 2016: The effect of improved chromatography on
1205   GDGT-based palaeoproxies. Organic Geochemistry 93, 1-6, doi: 10.1016/j.orggeochem.2015.12.006.
1206 Hopmans, E.C., Weijers, J.W.H., Schefuß, E., Herfort, L., Sinninghe Damsté, J.S., Schouten, S., 2004: A novel
1207   proxy for terrestrial organic matter in sediments based on branched and isoprenoid tetraether lipids. Earth
1208   and Planetary Science Letters 224, 107-116.
1209 Huber, M., Nof, D., 2006. The ocean circulation in the southern hemisphere and its climatic impacts in the
1210   Eocene. Palaeogeography, Palaeoclimatology, Palaeoecology 231, 9–28.
1211 Huber, M., Caballero, R., 2011. The early Eocene equable climate problem revisited. Climate of the Past 7,
1212   603–633.
1213 Huck, C.E., van de Flierdt, T., Bohaty, S.M., Hammond, S.J., 2017. Antarctic climate, Southern Ocean
1214   circulation patterns, and deep water formation during the Eocene. Palaeoceanography 32, 674–691.
1215 Iakovleva, A.I., Brinkhuis, H., Cavagnetto, C., 2001. Late Paleocene–Early Eocene dinoflagellate cysts from the
1216   Turgay Strait, Kazakhstan; correlations across ancient seaways. Palaeogeography, Palaeoclimatology,
1217   Palaeoecology 172, 243–268.
1218 Iakovleva, A.I., Heilmann-Clausen, C., 2007. *Wilsonidium pechoricum* new species – a new dinoflagellate
1219   species with unusual asymmetry from the Paleocene/Eocene transition. Journal of Paleontology 8, 1020–
1220   1030.
1221 Inglis, G.N., Farnsworth, A., Lunt, D., Foster, G.L., Hollis, C.J., Pagani, M., Jardine, P.E., et al., 2015: Descent
1222   toward the Icehouse: Eocene sea surface cooling inferred from GDGT distributions. Paleoceanography 29
1223   doi: 10.1002/2014PA002723.
1224 Jiang, S., Wise, S.W., 2009. Distinguishing the influence of diagenesis on the paleoecological reconstruction of
1225   nannoplankton across the Paleocene/Eocene Thermal Maximum: an example from the Kerguelen Plateau,
1226   southern Indian Ocean. Marine Micropaleontology 72, 49–59.
1227 Kershaw, A.P., 1970. Pollen morphological variation within the Casuarinaceae. Pollen et Spores 12, 145–161.
1228 Kim, J.-H., van der Meer, J., Schouten, S., Helmke, P., Willmott, V., Sangiorgi, F., Koç, N., et al., 2010. New
1229   indices and calibrations derived from the distribution of crenarchaeal isoprenoid tetraether lipids:
1230   Implications for past sea surface temperature reconstructions. Geochimica et Cosmochimica Acta 74, 4639-
1231   4654, doi: 10.1016/j.gca.2010.05.027.
1232 Kirtland Turner, S., Sexton, P.F., Charles, C.D., Norris, R.D., 2014. Persistence of carbon release events
1233   through the peak of early Eocene global warmth. Nature Geoscience 7, 748–751.

1234 Köthe, A., 1990. Paleogene dinoflagellates from northwest Germany: biostratigraphy and paleoenvironment.
1235   Geol. Jahrb. A 118, 3–111.
1236 Lauretano, V., Littler, K., Polling, M., Zachos, J.C., Lourens, L.J., 2015. Frequency, magnitude and character of
1237   hyperthermal events at the onset of the Early Eocene Climatic Optimum. Climate of the Past 11, 1313–1324.
1238 Lauretano, V., Hilgen, F.J., Zachos, J.C., Lourens, L.J., 2016. Astronomically tuned age model for the early
1239   Eocene carbon isotope events: A new high resolution $\delta^{13}C_{benthic}$ record of ODP Site 1263 between ~49 and
1240   ~54 Ma. Newsletters on Stratigraphy 49, 383–400.
1241 Lauretano, V., Zachos, J.C., Lourens, L.J., 2018. Orbitally paced carbon and deep-sea temperature changes at
1242   the peak of the Early Eocene Climatic Optimum. Paleoceanography and Paleoclimatology 33, 1050–1065,
1243   doi: 10.1029/2018PA003422.
1244 Littler, K., Röhl, U., Westerhold, T., Zachos, J.C., 2014. A high-resolution benthic stable-isotope record for the
1245   South Atlantic: Implications for orbital-scale changes in late Paleocene–Early Eocene climate and carbon
1246   cycling. Earth and Planetary Science Letters 401, 18–30.
1247 Lunt, D.J., Dunkley Jones, T., Heinemann, M., Huber, M., LeGrande, A., Winguth, A., Loptson, C., Marotzke,
1248   J., Roberts, C.D., Tindall, J., Valdes, P., Winguth, C., 2012. A model-data comparison for a multi-model
1249   ensemble of ealy Eocene atmosphere-ocean simulations: EoMIP. Climate of the Past 8, 1717–1736.
1250 Lunt, D.J., Huber, M., Anagnostou, E., Baatsen, M., Caballero, R.m DeConto, R., Dijkstra, H., Donnadieu, Y.,
1251   Evans, D., et al., 2017. The DeepMIP contribution to PMIP4: experimental design for model simulations of
1252   the EECO, PETM and pre-PETM (version 1.0). Geoscientific Model Devlopment 10, 889–901.
1253 Macphail, M.K., Alley, N.F., Truswell, E.M., Sluiter, I.R.K., 1994: Early Tertiary vegetation: evidence from
1254   spores and pollen. *In*: Hill, R.S. (ed.), History of the Australian vegetation: Cretaceous to Recent. Cambridge
1255   University Press, p. 189–261.
1256 Martini, E., 1971. Standard Tertiary and Quaternary calcareous nannoplankton zonation. Paper presented at the
1257   Proceedings of the Second Planktonic Conference, Roma.
1258 Matthews, K., Maloney, K., Zahirovic, S., Williams, S., Seton, M., Müller, D., 2016. Global plate boundary
1259   evolution and kinematics since the late Paleozoic. Global and Planetary Change 146, 226–250.
1260 McGowran, B., Hill, R.S., 2015: Cenozoic climate shifts in southern Australia. Transactions of the Royal
1261   Society of South Australia 139, 19–37.
1262 McIntyre, A., Bé, A.W.H., 1967. Modern Coccolithophoridae of the Atlantic Ocean. I. Placoliths and cyrtoliths.
1263   Deep Sea Research 14, 561–597.
1264 Morgans, H.E.G., Beu, A.G., Cooper, R.A., Crouch, E.M, Hollis, C.J., Jones, C.M., Raine, J.I., Strong, C.P.,
1265   Wilson, G.J., Wilson, G.S., 2004: Chapter 11, Paleogene (Dannevirke, Arnold and Landon Series). *In*:
1266   Cooper, R.A. (ed.), The New Zealand Geological Timescale. Institute of Geological and Nuclear Sciences
1267   Monograph 22, p. 125–163.
1268 Morgans, H.E.G., Jones, C., Crouch, E.M, Field, B.D., Raine, J.I., Strong, C.P., Wilson, G.J., 2005. Upper
1269   Cretaceous to Eocene stratigraphy and sample collections, mid-Waipara River, North Canterbury. Institute
1270   of Geological and Nuclear Sciences report 2003/08. 101p.
1271 Naafs, B.D.A., Pancost, R.D., 2016. Sea-surface temperature evolution across Aptian Oceanic Anoxic Event 1a.
1272   Geology 44, 959-962, doi: 10.1130/G38575.1.
1273 Naafs, B.D.A., Gallego-Sala, A.V., Inglis, G.N., Pancost, R.D., 2017a. Refining the global branched glycerol
1274   dialkyl glycerol tetraether (brGDGT) soil temperature calibration. Organic Geochemistry 106, 48-56, doi:
1275   10.1016/j.orggeochem.2017.01.009.
1276 Naafs, B.D.A., Inglis, G.N., Zheng, Y., Amesbury, M.J., Biester, H., Bindler, R., Blewett, J., et al., 2017b.
1277   Introducing global peat-specific temperature and pH calibrations based on brGDGT bacterial lipids.
1278   Geochimica et Cosmochimica Acta 208, 285-301, doi: 10.1016/j.gca.2017.01.038.
1279 Naafs, B.D.A., Rohrssen, M., Inglis, G., Lähteenoja, O., Feakins, S., Collinson, M., Kennedy, E., Singh, P.,
1280   Lunt, D., Pancost, R.D., 2018. High temperatures in the terrestrial mid-latitudes during the early Paleogene.
1281   Nature Geoscience 11, 766–771, doi:10.1038/s41561-018-0199-0.
1282 Nicolo, M.J., Dickens, G.R., Hollis, C.J., Zachos, J.C., 2007. Multiple early Eocene hyperthermals: Their
1283   sedimentary expression on the New Zealand continental margin and in the deep sea. Geology 35, 699–702.
1284 O'Brien, C., Robinson, S., Pancost, R., Sinninghe Damsté, J., Schouten, S., Lunt, D., Alsenz, H., Bornemann,
1285   A., Bottini, C., Brassell, S., Farnsworth, A., Forster, A., Huber, B., Inglis, G., Jenkyns, H., Linnert, C.,
1286   Littler, K., Markwick, P., McAnena, A., Mutterlose, J., Naafs, B.D.A., Püttmann, W., Sluijs, A., van
1287   Helmond, N.A.G.M., Vellekoop, J., Wagner, T., Wrobel, N., 2017. Cretaceous sea-surface temperature
1288   evolution: Constraints from TEX_{86} and planktonic foraminiferal oxygen isotopes. Earth-Science Reviews
1289   172, 224-247, doi: 10.1016/j.earscirev.2017.07.012.
1290 Okado, H., Honjo, S., 1973. The distribution of oceanic coccolithophorids in the Pacific. Deep Sea Research 20,
1291   355–374.

Pälike, H., Lyle, M. (editors), 2010. Methods (Expedition 320/321 Scientists), *In* Proceedings of the Integrated Ocean Drilling Program, 320/321.

Pancost, R.D., Taylor, K., Inglis, G.N., Kennedy, E.M., Handley, L., Hollis, C.J., Crouch, E.M., Pross, J., Huber, M., Schouten, S., Pearson, P.N., Morgans, H.E.G., Raine, J.I., 2013. Early Paleogene evolution of terrestrial climate in the SW Pacific, Southern New Zealand. Geochemistry, Geophysics, Geosystems 14, doi:10.1002/2013GC004935.

Pearson, P.N., van Dongen, B., Nicholas, C.J., Pancost, R.D., Schouten, S., Singano, J., Wade, B., 2007. Stable warm tropical climate throug the Eocene Epoch. Geology 35, 211–214.

Perch-Nielsen, K., 1985. Cenozoic calcareous nannofossils. *In* Bolli, H., Perch-Nielsen, K., et al. (eds.), Plankton Stratigraphy (pp. 427–554). New York: Cambridge University Press.

Pocknall, D.T., 1990: Palynological evidence for the early and middle Eocene vegetation and climate history of New Zealand. Review of Palaeobotany and Palynology 65, 57–69.

Prasad, V., Garg, R., Khowaja-Ateequzzaman, Singh, I.B., Joachimski, M., 2006. *Apectodinium* acme and palynofacies characteristics in the latest Paleocene–earliest Eocene of northeastern India: biotic response to the Paleocene–Eocene thermal maxima (PETM) in low latitude. Journal of The Paleontological Society of India 51, 75–91.

Prebble, J.G., Crouch, E.M., Carter, L., Cortese, G., Bostok, H., Neil, H., 2016. An epanded modern dinoflagellate cyst dataset for the Southwest Pacific and Southern Hemisphere with environmental associations. Marine Micropaleontology 101, 33–48.

Prebble, J.G., Crouch, E.M., Cortese, G., Carter, L., Neil, H., Bostok, H., 2016. Southwest pacific sea surface conditions during Marine Isotope Stage 11 – Results from dinoflagellate cysts. Palaeogeography, Palaeoclimatology, Palaeoecology 446, 19–31.

Prider, J.N., Christophel, D.C., 2000: Distributional ecology of *Gymnostoma australianum* (Casuarinaceae), a putative palaeoendemic of Australian wet tropic forsts. Australian Journal of Botany 48, 427–434.

Pross, J., Schmiedl, G., 2002. Early Oligocene dinoflagellate cysts from the Upper Rhine Graben (SW Germany): paleoenvironmental and paleoclimatic implications. Marine Micropaleontology 45, 1–24.

Raine, J.I., 1984: Outline of a palynological zonation of Cretaceous to Paleogene terrestrial sediments in the West Coast region, South Island. New Zealand Geological Survey report 109. 82 p.

Raine, J.I., Kennedy, E.M., Crouch, E.M., 2009: New Zealand Paleogene vegetation and climate. *In* Crouch, E., Strong, C.P., Hollis, C. (eds.), Climatic and Biotic Events of the Paleogene (CBEP), extended abstracts from an international conference in Wellington, New Zealand. GNS Science Miscellaneous Series 18, 117–122.

Raine, J.I., Beu, A.G., Boyes, A., Campbell, H.J., Cooper, R.A., Crampton, J.S., Crundwell, M., Hollis, C.J., Morgans, H.E.G., Mortimer, N., 2015. New Zealand Geological Timescale NZGT 2015/1. New Zealand Journal of Geology and Geophysics 58, 398–403.

Reay, M., 1993. Geology of the middle part of the Clarence Valley. Institute of Geological and Nuclear Sciences Geological Map 10, 1-144.

Reichart, G.-J., Brinkhuis, H., Huiskamp, F., Zachariasse, W.J., 2004. Hyperstratification following glacial overturning events in the northern Arabian Sea. Paleoceanography 19, PA2013, doi:10.1029/2003PA000900.

Schmitz, B., Pujalte, V., 2007. Abrupt increase in seasonal extreme precipitation at the Paleocene–Eocene boundary. Geology 35, 215–218.

Schneider, L. J., Bralower, T. J., Kump, L. R., 2011. Response of nannoplankton to early Eocene ocean destratification. Palaeoceanography, Palaeoclimatology, Palaeoecology 310, 152–162.

Schouten, S., Hopmans, E.C., Schefuss, E., Sinninghe Damsté, J.S., 2002. Distributional variations in marine crenarchaeotal membrane lipids: a new tool for reconstructing ancient sea water temperatures? Earth and Planetary Science Letters 204, 265-274, doi: 10.1016/S0012-821X(02)00979-2.

Schouten, S., Forster, A., Panato, F., Sinninghe Damsté, J.S., 2007. Towards calibration of the TEX$_{86}$ palaeothermometer for tropical sea surface temperatures in ancient greenhouse worlds. Organic Geochmistry 38, 1537–1546, doi: 10.1016/j.orggeochem.2007.05.014.

Shamrock, J. L., Watkins, D. K., 2012. Eocene calcareous nannofossil biostratigraphy and community structure from Exmouth Plateau, Eastern Indian Ocean (ODP Site 762). Stratigraphy 9. 54 pp.

Shepherd, C. L., 2017. Early to middle Eocene calcareous nannofossils of the SW Pacific: Paleobiogeography and paleoclimate (Unpublished doctoral thesis). Victoria University of Wellington, Wellington, New Zealand. 171 p.

Shepherd, C. L., Kulhanek, D. K., 2016. Eocene nannofossil biostratigraphy of the mid-Waipara River section, Canterbury Basin, New Zealand. Journal of Nannoplankton Research 36, 33–59.

Siesser, W.G., 1993. Calcareous nannoplankton. *In* Lipps, J.H. (ed.), Fossil Prokaryotes and Protists. Blackwell Scientific Publications, 169–201.

1350 Sinninghe Damsté, J.S., Schouten, S., Hopmans, E.C., van Duin, A.C.T., Geenevasen, J., 2002. Crenarchaeol:
1351   the characteristic core glycerol dibiphytanyl glycerol tetraether membrane lipid of cosmopolitan pelagic
1352   crenarchaeota. Journal of Lipid Research 43, 1641-1651, doi: 10.1194/jlr.M200148-JLR200.
1353 Sinninghe Damsté, J.S., 2016. Spatial heterogeneity of sources of branched tetraethers in shelf systems: The
1354   geochemistry of tetraethers in the Berau River delta (Kalimantan, Indonesia). Geochimica et Cosmochimica
1355   Acta 186, 13-31.
1356 Slimani, H., Guédé, K. E., Williams, G.L., Asebriy, L., Ahmamou, M., 2016. Campanian to Eocene
1357   dinoflagellate biostratigraphy from the Tahar and Sekada sections at Arba Ayacha, western External Rif,
1358   Morocco. Review of Palaeobotany and Palynology 228, 26–46.
1359 Slotnick, B.S., Dickens, G.R., Nicolo, M.J., Hollis, C.J., Crampton, J.S., Zachos, J.C., Sluijs, A., 2012. Large-
1360   amplitude variations in carbon cycling and terretrial weathering during the Latest Paleocene and Earliest
1361   Eocene: the record at Mead Stream, New Zealand. The Journal of Geology 120, 487–505.
1362 Slotnick, B.S., Dickens, G.R., Hollis, C.J., Crampton, J.S., Strong, C.P., Phillips, A., 2015. The onset of the
1363   Early Eocene Climatic Optimum at Branch Stream, Clarence River valley, New Zealand. New Zealand
1364   Journal of Geology and Geophysics 58, 262–280.
1365 Sluijs, A., Pross, J., Brinkhuis, H., 2005. From greenhouse to icehouse; organic-walled dinoflagellate cysts as
1366   paleoenvironmental indicators in the Paleogene. Earth-Science Reviews 68, 281–315.
1367 Sluijs, A., Brinkhuis, H., 2009. A dynamic climate and ecosystem state during the Paleocene–Eocene Thermal
1368   Maximum: inferences from dinoflagellate cyst assemblages on the New Jersey Shelf. Biogeosciences 6,
1369   1755–1781.
1370 Steane, D.A., Wilson, K.L., Hill, R.S., 2003. Using *mat*K sequence data to unravel the phyology of
1371   Casuarinaceae. Molecular Phylogenetics and Evolution 28, 47–59.
1372 Taylor, K.W.R., Huber, M., Hollis, C.J., Hernandez-Sanchez, M.T., Pancost, R.D., 2013. Re-evaluating modern
1373   and Palaeogene GDGT distributions: Implications for SST reconstructions. Global and Planetary Change
1374   108, 158-174, doi: 10.1016/j.gloplacha.2013.06.011.
1375 Taylor, K.W.R., Willumsen, P.S., Hollis, C.J., Pancost, R.D., 2018. South pacific evidence for the long-term
1376   climate impact of the Cretaceous/Paleogene boundary event. Earth-Science Reviews 179, 287–302.
1377 Tierney, J.E., Tingley, M.P., 2014. A Bayesian, spatially-varying calibration model for the TEX_{86} proxy.
1378   Geochimica et Cosmochimica Acta 127, 83-106, doi: 10.1016/j.gca.2013.11.026.
1379 Tierney, J.E., Tingley, M.P., 2015. A TEX_{86} surface sediment database and extended Bayesian calibration.
1380   Scientific Data 2, 150029, doi: 10.1038/sdata.2015.29.
1381 Tierney, J.E., Sinninghe Damsté J., S., Pancost, R.D., Sluijs, A., Zachos, J.C., 2017. Eocene temperature
1382   gradients. Nature Geoscience 10, 538-539.
1383 Trommer, G., Siccha, M., van der Meer, M.T.J., Schouten, S., Sinninghe Damsté, J.S., Schulz, H., Hemleben,
1384   C., et al., 2009. Distribution of Crenarchaeota tetraether membrane lipids in surface sediments from the Red
1385   Sea. Organic Geochemistry 40, 724-731, doi: 10.1016/j.orggeochem.2009.03.001.
1386 Van Hinsbergen, D., de Groot, L., van Schaik, J., Spakman, W., Bijl, P., Sluijs, A., Langereis, C., Brinkhuis, H.,
1387   2015. A Paleolatitude Calculator for Paleoclimate Studies, PLOS ONE, 10, 10.1371/journal. pone.0126946.
1388 Villa, G., Persico, D., 2006. Late Oligocene climatic changes: Evidence from calcareous nannofossils at
1389   Kerguelen Plateau Site 748 (Southern Ocean). Palaeogeography, Palaeoclimatology, Palaeoecology 231,
1390   110–119, doi: 10.1016/j.palaeo.2005.07.028.
1391 Villa, G., Fioroni, C., Pea, L., Bohaty, S., Persico, D., 2008. Middle Eocene–late Oligocene climate variability:
1392   Calcareous nannofossil response at Kerguelen Plateau, Site 748. Marine Micropaleontology 69, 173–192,
1393   doi: 10.1016/j.marmicro.2008.07.006.
1394 Wei, W., Wise, S. W., 1990. Biogeographic gradients of middle Eocene–Oligocene calcareous nannoplankton in
1395   the South Atlantic Ocean. Palaeogeography, Palaeoclimatology, Palaeoecology 79, 29–61, doi:
1396   10.1016/0031-0182(90)90104-F.
1397 Weijers, J.W.H., Schouten, S., Hopmans, E.C., Geenevasen, J.A.J., David, O.R.P., Coleman, J.M., Pancost,
1398   R.D., et al., 2006. Membrane lipids of mesophilic anaerobic bacteria thriving in peats have typical archaeal
1399   traits. Environmental Microbiology 8, 648-657, doi: 10.1111/j.1462-2920.2005.00941.x.
1400 Weijers, J.W.H., Schouten, S., van den Donker, J.C., Hopmans, E.C., Sinninghe Damsté, J.S., 2007.
1401   Environmental controls on bacterial tetraether membrane lipid distribution in soils. Geochimica et
1402   Cosmochimica Acta 71, 703-713, doi: 10.1016/j.gca.2006.10.003.
1403 Westerhold, T., Röhl, U., 2009. High resolution cyclostratigraphy of the early Eocene – new insights into the
1404   origin of the Cenozoic cooling trend. Climate of the Past 5, 309–327.
1405 Westerhold, T., Röhl, U., Laskar, J., 2012. Time scale controversy: Accurate orbital calibration of the early
1406   Paleogene. Geochemistry, Geophysics, Geosystems 13, Q06015, doi:10.1029/2012GC004096.

1407 Westerhold, T., Röhl, U., Frederichs, T., Agnini, C., Raffi, I., Zachos, J.C., Wilkins, R.H., 2017. Astronomical
1408   calibration of the Ypresian Time Scale: Implications for seafloor spreading rates and the chaotic behaviour
1409   of the solar system? Climate of the Past 13, 1129–1152.
1410 Westerhold, T., Röhl, U., Donner, B., Zachos, J.C., 2018. Global extent of the Early Eocene hyperthermal
1411   events – a new Pacific benthic foraminiferal isotope record from Shatsky Rise (ODP site 1209).
1412   Paleoceanography and Paleoclimatology 33, 626–642, doi:10.1029/2017PA003306.
1413 Wilson, G.J., 1984. New Zealand Late Jurassic to Eocene dinoflagellate biostratigraphy – a summary.
1414   Newsletters on Stratigraphy 13, 104–117.
1415 Wilson, G.J., 1988. Paleocene and Eocene dinoflagellate cysts from Waipawa, Hawkes Bay, New Zealand. New
1416   Zealand Geological Survey Paleontological Bulletin 57. 96p.
1417 Wrenn, J.H., Beckman, S.W., 1982. Maceral, total organic carbon and palynological analyses of Ross Ice Shelf
1418   Project Site J9 cores. Science 216, 187–189, doi:10.1126/science.216.4542.187.
1419 Zachos, J.C., Pagani, M., Sloan, L., Thomas, E., Billups, K., 2001. Trends, rhythms, and aberrations in global
1420   climate 65 Ma to present. Science 292, 686–693.
1421 Zachos, J.C., Schouten, S., Bohart, S., Quattlebaum, T., Sluijs, A., Brinkhuis, H., Gibbs, S., Bralower, T., 2006.
1422   Extreme warming of mid-latitude coastal ocean during the Paleocene–Eocene Thermal Maximum:
1423   Inferences from TEX86 and isotope data. Geology 34, 737–740.
1424 Zachos, J.C., Dickens, G.R., Zeebe, R.E., 2008. An early Cenozoic perspective on greenhouse warming and
1425   carbon-cycle dynamics. Nature 45, 279–283.
1426 Zhang, Y.G., Zhang, C.L., Liu, X.-L., Li, L., Hinrichs, K., Noakes, J.E., 2011. Methane Index: A tetraether
1427   archaeal lipid biomarker indicator for detecting the instability of marine gas hydrates. Earth and Planetary
1428   Science Letters 307, 525–534.
1429 Zonneveld, K.A.F., Marret, F., Versteegh, G., Bogus, K., Bonnet, S., Bouimetarhan, I., Crouch, E.M., de
1430   Vernal, A., et al., 2013. Atlas of modern dinoflagellate cyst distribution based on 2045 data points. Review
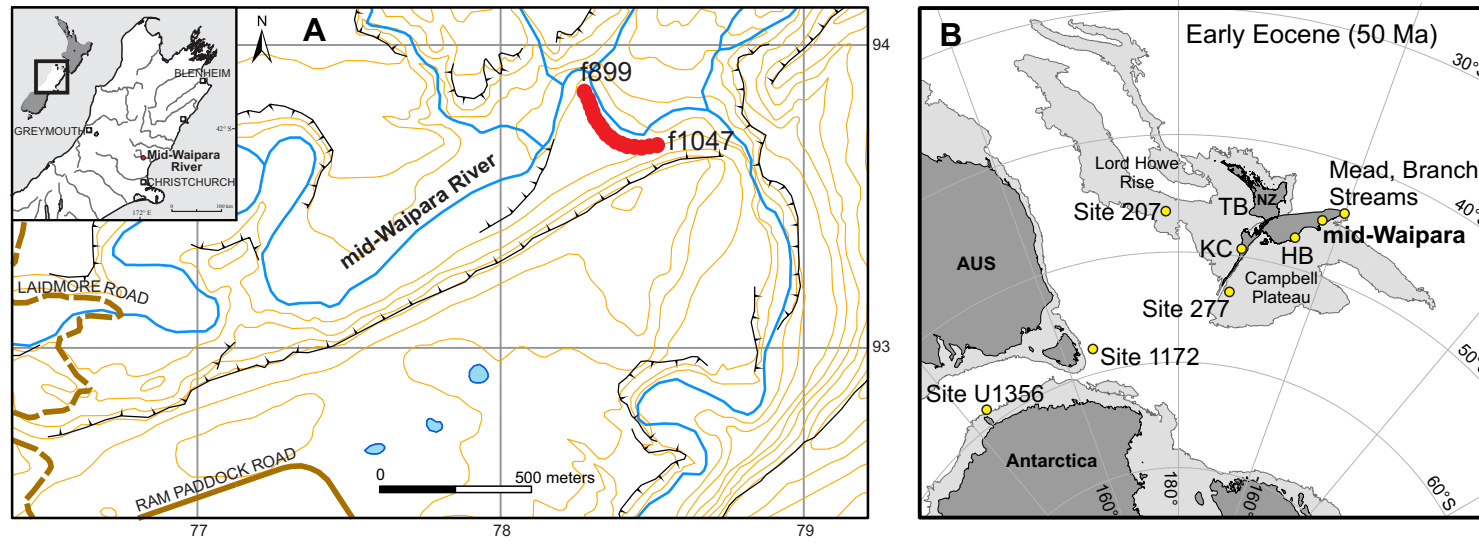1431   of Palaeobotany and Palynology 191, 1–197.
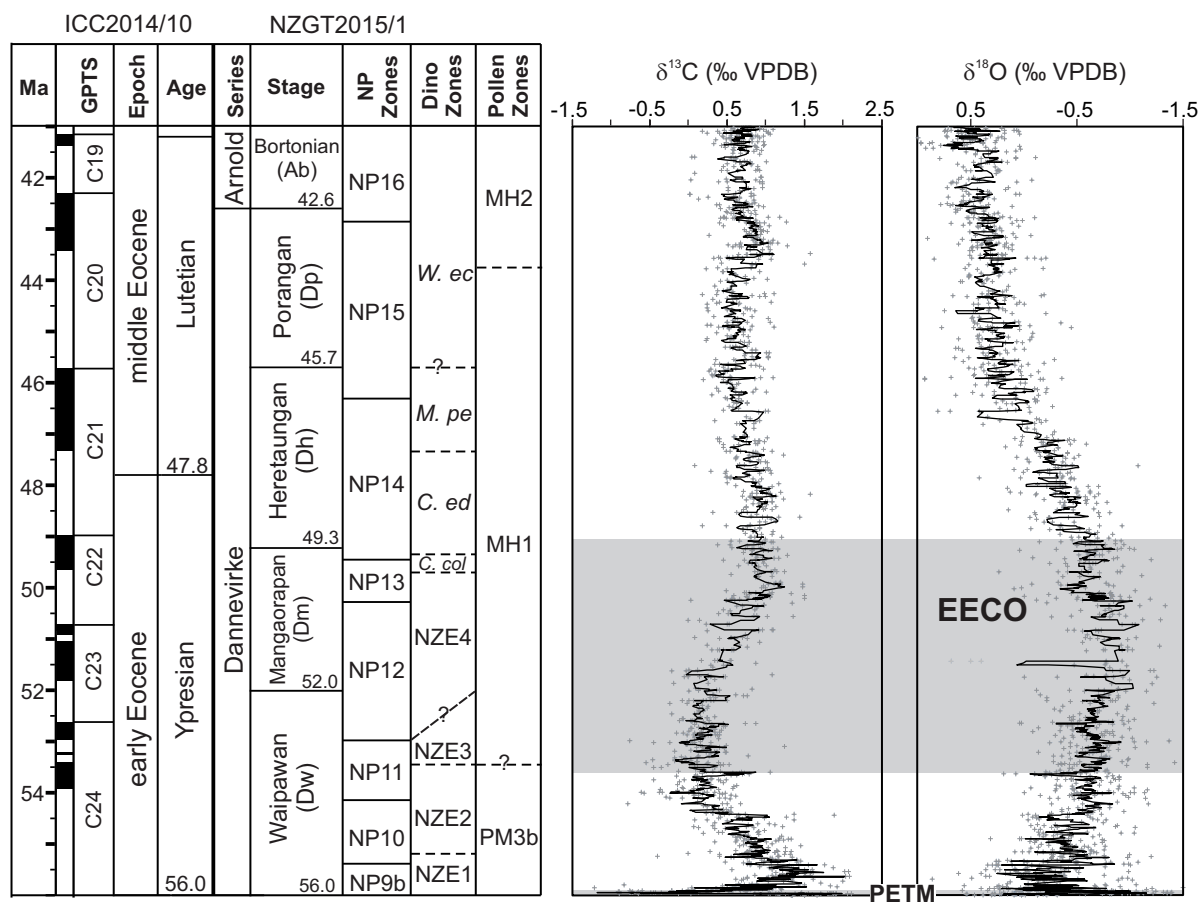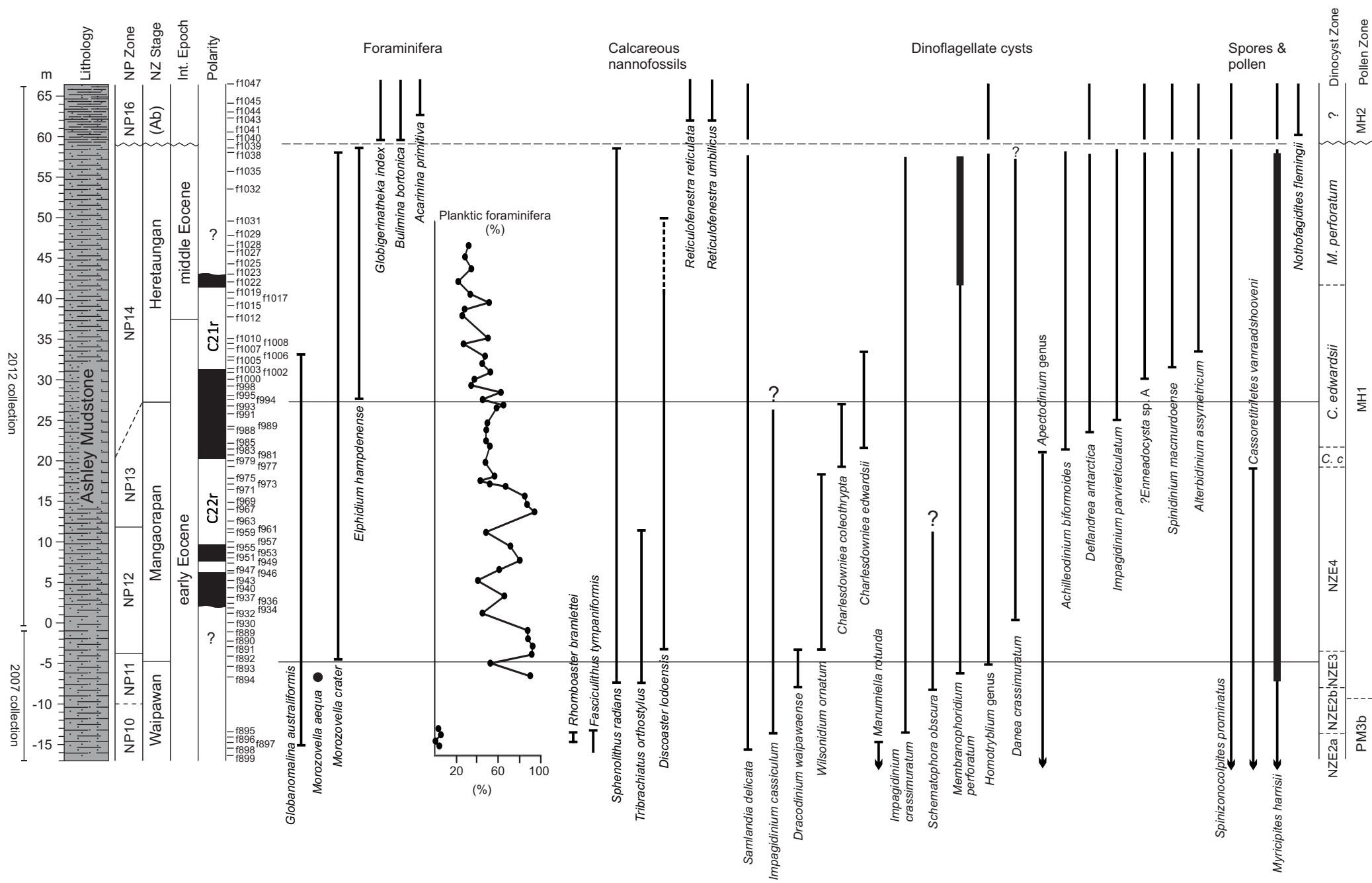1432

Figure 1

Figure 2

Figure 3
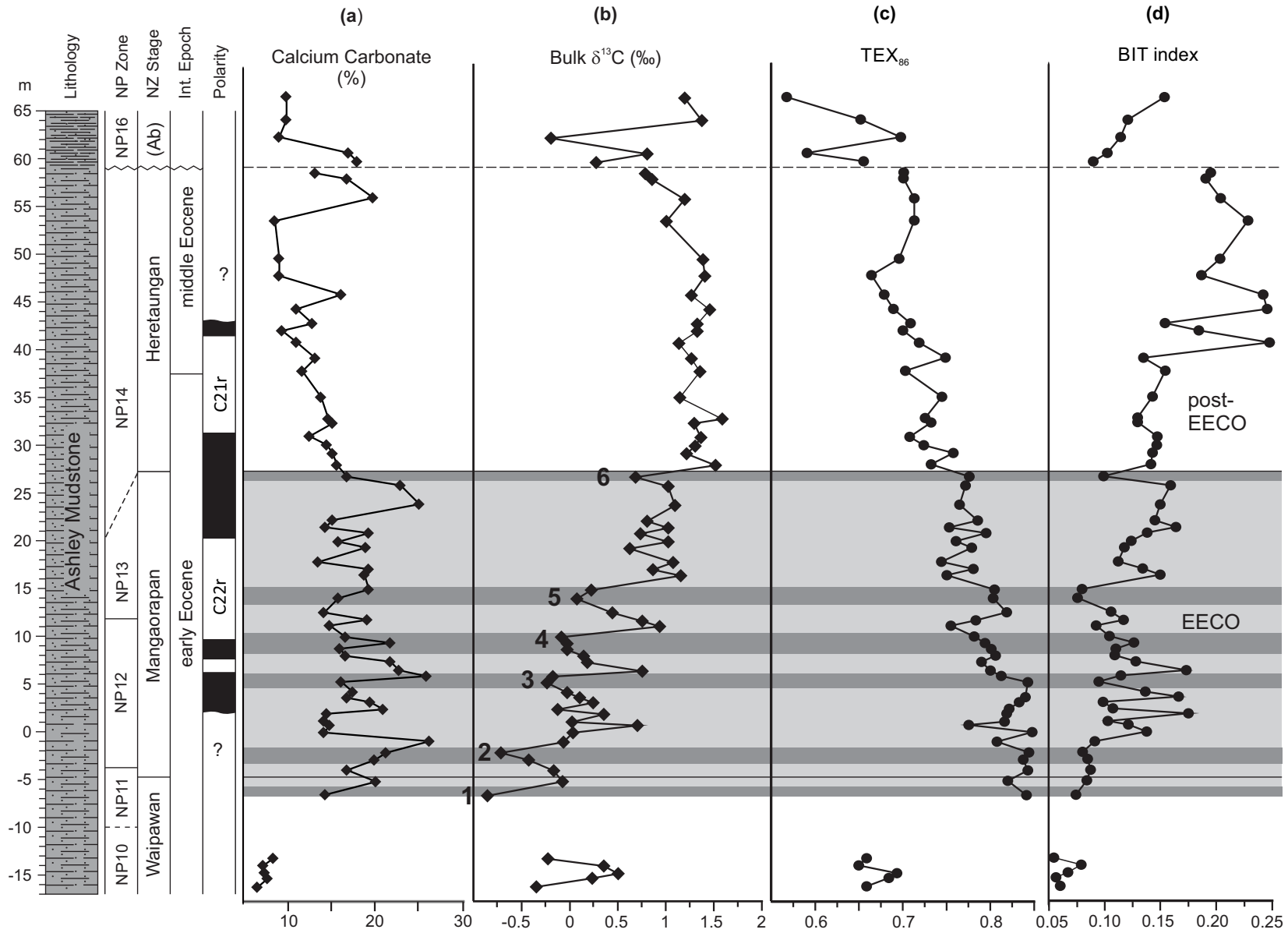
Figure 4

Figure 5

Figure 6

(a) Atlantic and Pacific Ocean
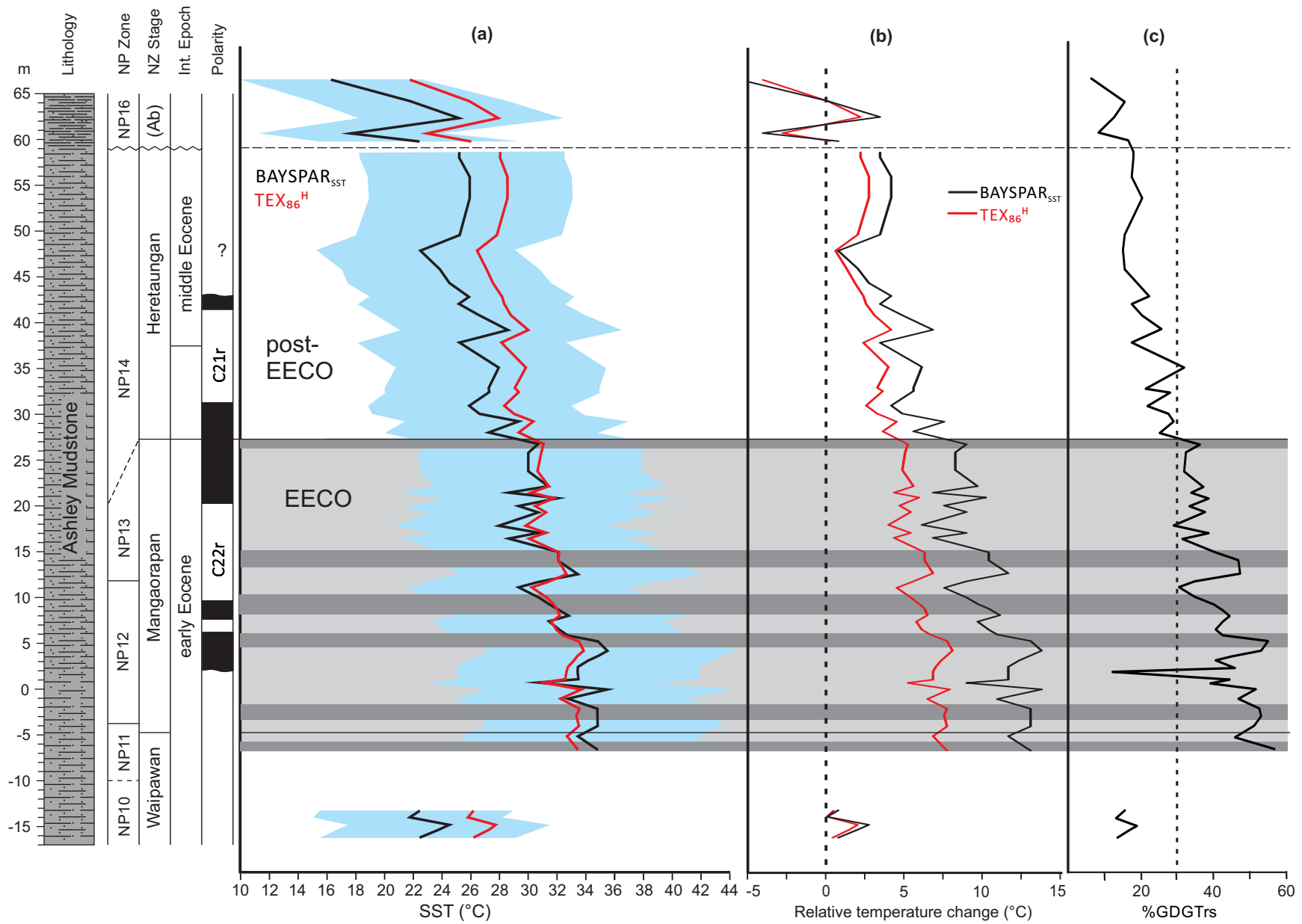
(b) mid-Waipara River
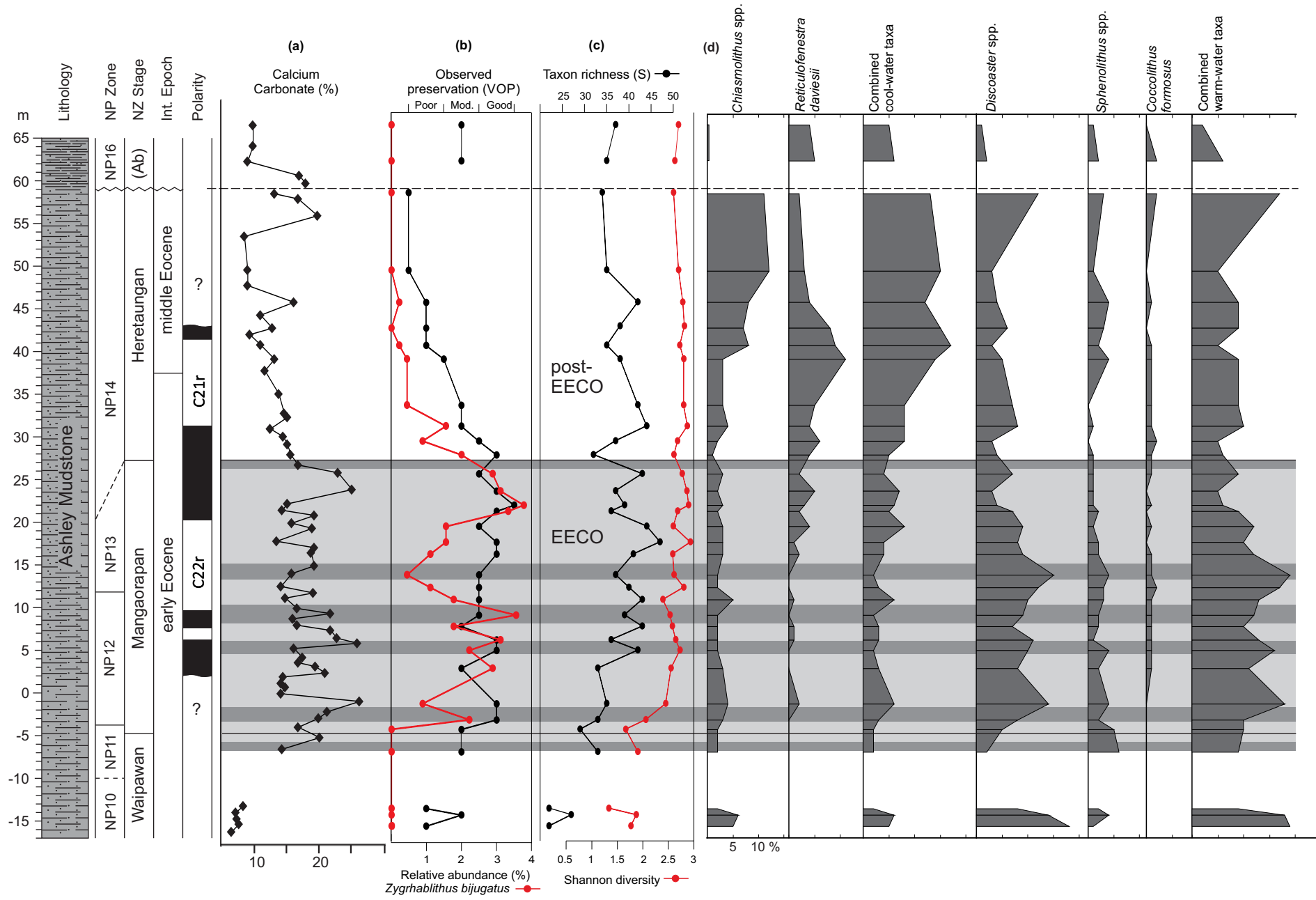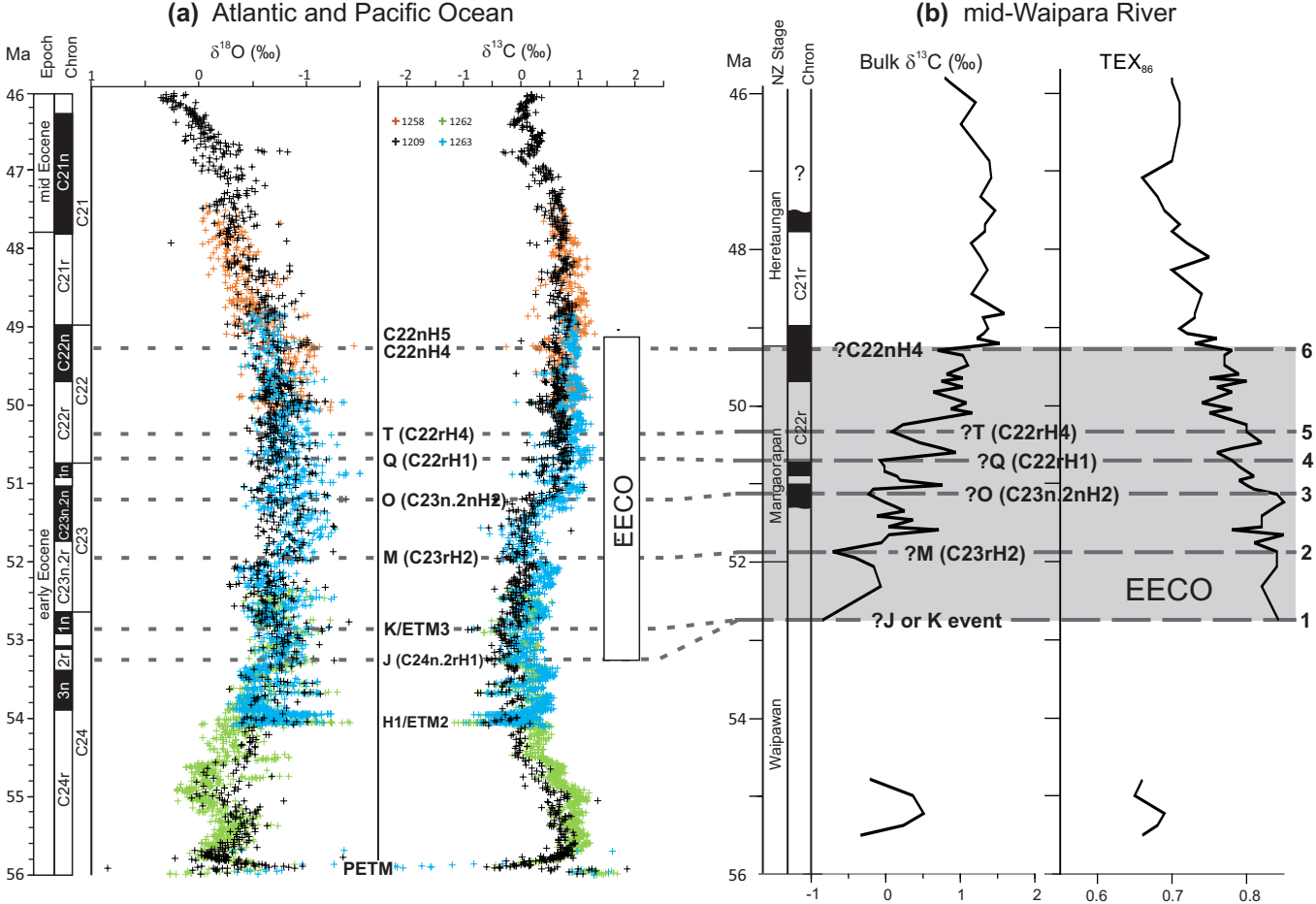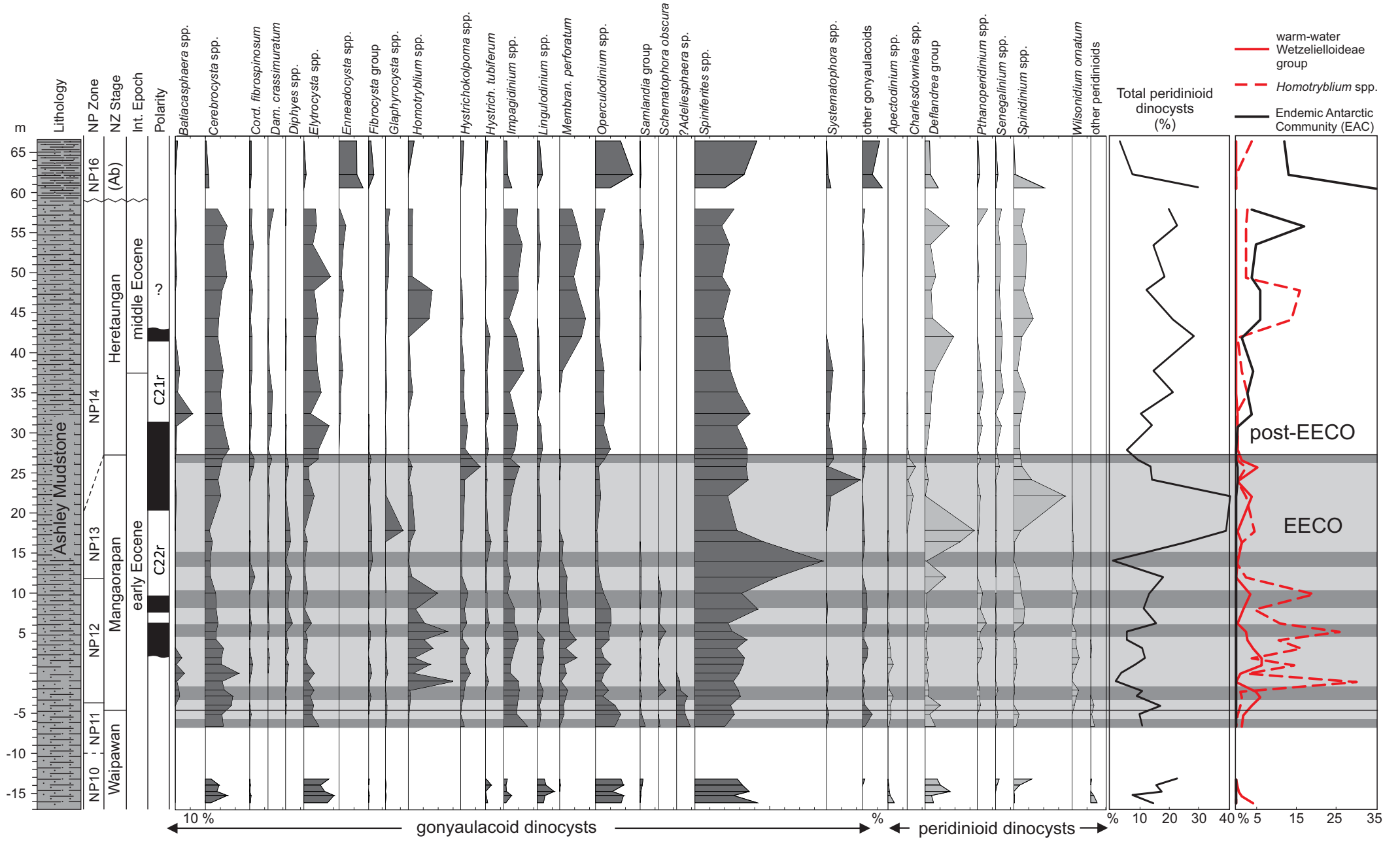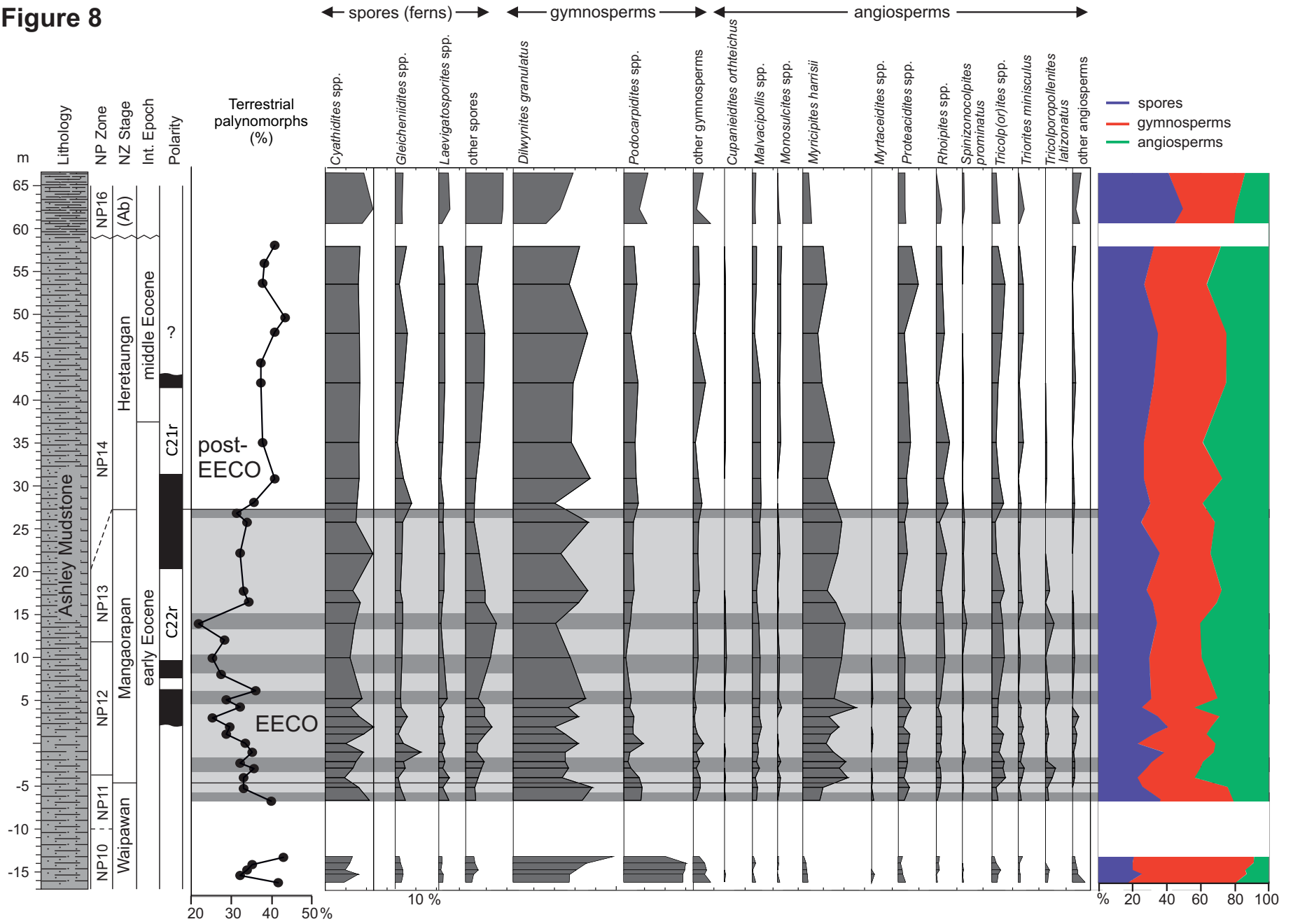
Figure 7

Figure 8

Figure 9

Figure 10

Figure 11

Figure 12